American Mineralogist, Volume 81, pages 561–584, 1996

# Microstructures and high-temperature phase transitions in kalsilite

MICHAEL A. CARPENTER AND DANIELA CELLAI

Department of Earth Sciences, University of Cambridge, Downing Street, Cambridge CB2 3EQ, U.K.

## ABSTRACT

A diversity of twinning and exsolution textures has been observed by transmission electron microscopy in natural kalsilite from volcanic and metamorphic rocks (Mount Nyiragongo, Zaire; Alban Hills, Italy; Kerala, southern India). The phase transitions responsible for these microstructures were examined by high-temperature powder and single-crystal X-ray diffraction. Pure kalsilite has $P6_3mc$ symmetry at high temperatures but transforms to its $P6_3$ state through a two-phase field, between ~870 and ~920 °C. In this two-phase field, the low form coexists with a structure that has a sixfold repeat of its $a$ unit-cell dimension. For $\sim Ks_{88}$, the high-temperature state is high tetrakalsilite with possible space group $P6_3mc$; a two-phase field between ~890 and ~930 °C involves the coexistence of this phase with $P6_3$ kalsilite. High tetrakalsilite with composition $\sim Ks_{74}$ reverts to low tetrakalsilite on quenching to room temperature from 950 °C. Lattice-parameter variations, and estimates of the Al-O-Si angles that can be derived from them, imply that the stability limit for the high structural states occurs when the angles for apical and basal O atoms converge. At lower temperatures, pure $P6_3$ kalsilite appears to have transformed during a metamorphic evolution in nature to an intergrowth of the $P6_3$ structure and a structure for which $P31c$ symmetry is proposed. The latter can be thought of as a polytype of kalsilite, with (001) layers stacked in an eclipsed array rather than in the staggered array of normal low kalsilite. In this regard, $KAlSiO_4$ seems to be remarkably similar to $KLiSO_4$. If ~3–12 mol% $NaAlSiO_4$ is present in solid solution, a $P6_3$ structure with an $a$ parameter $\sqrt{3}$ greater than normal low kalsilite develops. An anomaly in the lattice parameters of $Ks_{88}$ suggests that the transition temperature below which this superstructure develops may be ~500 °C. Natural nepheline exsolved from kalsilite displays merohedral twinning, which can be accounted for by a $P6_3mc \rightarrow P6_3$ transition during cooling. Transformation behavior in the Ne-Ks system may be explained, at least qualitatively, in terms of Na-K ordering between cavity sites, ordering of basal O atoms between two sites on either side of the mirror plane parallel to the $c$ axis of $P6_3mc$ structures, ordering of apical O atoms between three sites, and coupling between all these processes.

## INTRODUCTION

Kalsilite ($KAlSiO_4$) is a rock-forming feldspathoid that occurs mainly in K-rich silica-undersaturated lavas; it is also found in ejected blocks incorporated into pyroclastics and, rarely, in metamorphic rocks. It undergoes several phase transitions at high temperatures and displays a remarkable diversity of structures over a limited range of compositions at the Ks-rich end of the nepheline-kalsilite system. The first structure refinement, by Perrotta and Smith (1965), was of a volcanic crystal with Na:K ≈ 0.02:0.98 and space group $P6_3$ (low kalsilite). Perrotta and Smith explained the relatively large $R$ value for their refinement as the result of disorder of the O atoms. In particular, apical O atoms linking successive (001) layers have mean positions on the threefold axes but appear actually to be randomly distributed among three sites displaced off these axes. The intersheet Al-O-Si bond angles are reduced from the improbable value of 180° as a consequence. Synthetic $KAlSiO_4$ has $P6_3mc$ symmetry at 950 °C (high kalsilite; Kawahara et al. 1987), and a structural phase transition involving the symmetry change $P6_3mc \rightleftharpoons P6_3$ has been proposed for the end-member composition (Andou and Kawahara 1982; Abbott 1984; Kawahara et al. 1987). The driving energy for this transition must arise predominantly from the ordering of displacements of O atoms linking the bases of the $AlO_4$ and $SiO_4$ tetrahedra. However, Capobianco and Carpenter (1989) found that the transition occurs by means of an intermediate phase, which coexists with low kalsilite between ~850 and ~920 °C and is characterized by weak superstructure reflections. New data presented in this paper suggest that the intermediate phase is hexagonal and not orthorhombic as originally suggested.

Four other room-temperature variants of the stuffed tridymite form of kalsilite have been reported in the composition range $\sim Ne_{30}Ks_{70}$–$Ks_{100}$. Smith and Sahama (1957) observed diffuse reflections in diffraction patterns from crystals taken from a lava from Mount Nyiragongo, Zaire. The unit cell for this material is related to that of

0003–004X/96/0506–0561$05.00

pure kalsilite by a 30° rotation about the $c$ axis and an increase of the $a$ lattice dimension by a factor of $\sqrt{3}$. These reflections disappeared after heating to 600 °C, but their origin has not been studied in any detail. Tetrakalsilite (proper mineral name: panunzite) and trikalsilite are also known from volcanic rocks, and tetrakalsilite has been synthesized (Sahama 1957, 1962; Sahama and Smith 1957; Smith and Tuttle 1957; Tuttle and Smith 1958; Merlino et al. 1985; Bonaccorsi et al. 1988; Hovis et al. 1992). Both typically contain ~30 mol% Ne in solid solution. Finally, kalsilite crystals produced from nepheline by ion exchange in molten KCl can give diffraction patterns with weak or absent $hhl$, $l$ = odd reflections, which imply that the $P6_3mc$ structure might exist at room temperature. Dollase and Freeborn (1977) considered the high symmetry of these crystals to represent only the average structure of two $P6_3$ merohedral twins related by a mirror plane normal to the $a$ axis and intergrown on a fine scale. Kalsilite prepared by hydrothermal methods can have a similar domain structure according to Andou and Kawahara (1984), with the volume proportions of the domains varying from crystal to crystal.

The structures of kalsilite, tetrakalsilite, trikalsilite, and nepheline all have $P6_3$ symmetry at room temperature and are characterized by stacking of tridymite-like sheets of alternating $AlO_4$ and $SiO_4$ tetrahedra to give a repeat distance along the $c$ axis of ~8.6 Å (referred to subsequently in this paper as $C$). The $a$ lattice parameter is a multiple of the ~5.2 Å distance between the centers of sixfold rings in the ideal tridymite structure, referred to here as $A$. The unit cells of kalsilite, nepheline, trikalsilite, and tetrakalsilite then have $1A$, $2A$, $3A$, and $4A$, respectively, as their $a$ dimension. Details of the structures are subtly different, however (Merlino 1984). In the nepheline structure the six-membered rings are oval and nearly hexagonal in the proportion 3:1 (Buerger et al. 1954; Hahn and Buerger 1955; Dollase 1970; Foreman and Peacor 1970; Dollase and Peacor 1971), whereas in kalsilite they all have a ditrigonal shape (Perrotta and Smith 1965; Andou and Kawahara 1984). Trikalsilite and tetrakalsilite have three kinds of six-membered rings in their unit cells—hexagonal, ditrigonal, and oval—in the proportions 2:4:12 and 2:12:18, respectively (Merlino 1984). Another important difference between the structures is the stacking of the (001) layers, which are distorted relative to ideal expanded tridymite sheets. In the $2A$, $3A$, and $4A$ structures successive layers are stacked in an "eclipsed" conformation, with a marked $P6_3/m$ pseudosymmetry. In the $1A$, $P6_3$ structure they are stacked in a "staggered" conformation (Merlino 1984), which means that every layer is deformed in the same manner, but all the ditrigonal rings in one layer point in one direction and all the rings in the next layer point in the opposite direction. The $1A$, $P6_3mc$ structure at high temperatures has open hexagonal rings (Kawahara et al. 1987), with a mirror plane perpendicular to $c$ violated only by the Al-Si ordering scheme. There were some early suggestions of incomplete Al-Si order in nepheline (Dollase and Peacor 1971), but NMR spectroscopic data indicate high degrees of order in natural and synthetic samples (Lippmaa et al. 1980; Stebbins et al. 1986; Hovis et al. 1992), and it now seems unlikely that any of these phases have substantial tetrahedral site disorder.

The highest temperature polymorph is O1-$KAlSiO_4$, which has a different framework topology than tridymite (Gregorkiewitz and Schäfer 1980; Merlino 1984). Other types of topologies are possible (Merlino 1984; Palmer 1994), but kaliophilite is the only phase with a kalsilite composition in this group that has so far been found in nature (Bannister and Hey 1931; Lukesh and Buerger 1942; Barbieri et al. 1970; Cellai et al. 1992). It has a unit cell that is a multiple of the low kalsilite cell, but its microstructure and thermal expansion behavior are not consistent with the enlarged cell simply being a kalsilite superstructure (Cellai et al. 1992). Both O1-$KAlSiO_4$ and natural kaliophilite undergo what appear to be displacive phase transitions at high temperatures (Lange et al. 1986; Capobianco and Carpenter 1989; Cellai et al. 1992).

Common to all these structures are (1) the influence of O-atom positional disorder in determining sequences of phase transitions and (2) the role of Na-K ordering in stabilizing particular framework distortions. The basic stuffed tridymite structure appears to be unable to accommodate changes in stoichiometry and temperature without also undergoing changes in symmetry. A primary objective of the in situ high-temperature X-ray diffraction study described in this paper, as opposed to previous anneal and quench experiments, was to define the relationships between the known variants of the kalsilite structure more explicitly. Close analogies with the behavior of compounds described in the literature, such as $(Na,K)AlGeO_4$, $(Na,K)GaSiO_4$, $SrAl_2O_4$, and $KLiSO_4$, provide new insights into the nature of the $\sqrt{3}A$ superstructure of Smith and Sahama (1957) and have led to the discovery of a new kalsilite structure with a suggested space group of $P31c$. If there are so many possible phase transitions, the development of complex microstructures should be anticipated; natural and heat-treated samples have also been examined by transmission electron microscopy.

## Experimental details

### Powder diffraction

X-ray measurements were made with a multichannel CPS-120 diffractometer described in Salje et al. (1993), using Cu$K\alpha_1$ radiation and a quartz monochromator. The sample was supported on a strip of platinum, which was used for resistance heating. Temperature was monitored using a Pt-13%Rh thermocouple welded to the underside of the strip and calibrated against the $\beta \rightleftharpoons \alpha$ transition temperature (573 °C) of quartz mounted in the same configuration. The uncertainty of the temperature scale was estimated to be ±5 °C, but the stability was within 1 °C. All experiments were performed in air, and $Al_2O_3$ was used as an internal standard. Each powder diffraction

**TABLE 1.** Lattice parameters of kalsilite obtained at high temperatures during heating cycles

| Homogenized $Ks_{88}$ | | | | Metamorphic $Ks_{100}$ | | | |
|---|---|---|---|---|---|---|---|
| $T$ (°C) | $a$ (Å) | $c$ (Å) | $V$ (Å$^3$) | $T$ (°C) | $a$ (Å) | $c$ (Å) | $V$ (Å$^3$) |
| 25 | 5.153(1) | 8.657(2) | 199.05(4) | 25 | 5.160(1) | 8.717(1) | 201.00(2) |
| 25* | 5.151(1) | 8.659(2) | 198.97(4) | 25* | 5.161(4) | 8.706(1) | 200.85(2) |
| 98 | 5.158(1) | 8.662(2) | 199.59(4) | 98 | 5.168(1) | 8.712(1) | 201.50(2) |
| 147 | 5.162(1) | 8.664(2) | 199.94(5) | 147 | 5.174(1) | 8.709(1) | 201.87(2) |
| 196 | 5.166(1) | 8.665(3) | 200.24(5) | 196 | 5.178(1) | 8.706(1) | 202.15(2) |
| 245 | 5.171(1) | 8.668(2) | 200.69(4) | 245 | 5.184(1) | 8.700(1) | 202.47(2) |
| 294 | 5.176(1) | 8.668(2) | 201.10(4) | 294 | 5.189(1) | 8.697(1) | 202.81(2) |
| 343 | 5.180(1) | 8.669(2) | 201.45(4) | 343 | 5.194(1) | 8.693(1) | 203.13(3) |
| 392 | 5.185(1) | 8.669(2) | 201.86(4) | 392 | 5.199(1) | 8.690(1) | 203.43(2) |
| 441 | 5.191(1) | 8.671(2) | 202.33(4) | 441 | 5.204(1) | 8.687(1) | 203.73(2) |
| 490 | 5.196(1) | 8.672(3) | 202.76(6) | 490 | 5.208(1) | 8.685(1) | 204.02(2) |
| 539 | 5.203(1) | 8.670(2) | 203.27(5) | 539 | 5.212(1) | 8.686(1) | 204.32(2) |
| 588 | 5.209(1) | 8.670(2) | 203.75(4) | 578 | 5.216(1) | 8.685(1) | 204.61(2) |
| 637 | 5.214(1) | 8.668(1) | 204.06(3) | 627 | 5.221(1) | 8.683(1) | 204.97(2) |
| 686 | 5.217(1) | 8.666(2) | 204.29(3) | 676 | 5.227(1) | 8.681(1) | 205.40(2) |
| 734 | 5.221(1) | 8.664(1) | 204.56(4) | 725 | 5.232(1) | 8.679(1) | 205.75(2) |
| 783 | 5.226(1) | 8.663(2) | 204.91(4) | 783 | 5.239(1) | 8.675(2) | 206.20(3) |
| 832 | 5.232(1) | 8.659(2) | 205.24(4) | 813 | 5.243(1) | 8.671(1) | 206.47(3) |
| 852 | 5.234(1) | 8.658(2) | 205.42(4) | 842 | 5.248(1) | 8.672(1) | 206.88(2) |
| 25** | 5.150(1) | 8.651(2) | 198.66(5) | 25** | 5.159(1) | 8.720(1) | 201.02(2) |
| 25*,** | 5.153(1) | 8.663(2) | 199.23(4) | 25*,** | 5.161(1) | 8.705(2) | 200.75(3) |
| 874** | 5.237(1) | 8.658(2) | 205.61(4) | 850** | 5.249(1) | 8.674(2) | 206.93(4) |
| 888** | 5.239(1) | 8.658(2) | 205.77(4) | 869** | 5.251(1) | 8.673(2) | 207.08(3) |
| 903** | 5.242(1) | 8.661(3) | 206.09(5) | 888** | 5.255(1) | 8.673(1) | 207.40(3) |
| 913** | 5.243(1) | 8.659(4) | 206.14(5) | 898** | 5.255(1) | 8.673(2) | 207.37(4) |
| 922** | 5.253(1) | 8.658(2) | 206.93(4) | 908** | 5.266(2) | 8.671(3) | 208.21(8) |
| 932** | 5.256(1) | 8.657(2) | 207.12(3) | 927** | 5.275(1) | 8.667(2) | 208.88(5) |
| 942** | 5.260(1) | 8.653(1) | 207.35(3) | 956** | 5.282(1) | 8.662(2) | 209.28(4) |
| 966** | 5.264(1) | 8.651(2) | 207.59(4) | 995** | 5.289(1) | 8.658(2) | 209.77(4) |
| 990** | 5.270(1) | 8.646(2) | 207.94(4) | | | | |
| 1024** | 5.281(1) | 8.638(2) | 208.63(4) | | | | |
| 1062** | 5.288(1) | 8.635(2) | 209.07(5) | | | | |

*Note:* Figures in parentheses indicate the uncertainty ($\pm 1\ \sigma$) in the last digit. The data were collected using two batches of sample.
* Lattice parameters obtained from data collected at room temperature after quenching from high temperature at the end of the full heating cycle.
** Data collected using the second batch of sample.

spectrum took 4–5 h to collect. Lattice parameters were determined by least-squares refinement using 20 reflections. A representative set of cell parameters as a function of temperature is given in Table 1.

### Single-crystal X-ray diffraction

Single-crystal X-ray diffraction experiments were conducted on a Philips PW1000 four-circle diffractometer with graphite-monochromatized Mo$K\alpha$ radiation. High temperatures were achieved using a horseshoe-shaped electrical resistance furnace, with the thermocouple situated about 5 mm from the crystal. For temperature calibration, the melting points of five samples were measured (Cellai et al. 1994). The uncertainty is ±15 °C for temperatures <600 °C. At higher temperatures we claim no better than ±30 °C for absolute temperatures. Intensity measurements of selected *hhl* reflections of kalsilite, and of superstructure reflections that correspond to fourfold or sixfold multiples of $A$, were collected from room temperature to ~1000 °C. The integrated intensities were measured using an $\omega$-$2\theta$ scan through 2° across the diffraction peak at a speed of 0.005°/s. Background intensities were measured on either side of the peak, and a linear interpolation was used to calculate the total background. Peak profiles were measured to check whether the reflections became diffuse with increasing temperature; a least-squares fit was performed using a Gaussian diffraction profile to determine the peak width.

### Transmission electron microscopy

TEM samples were prepared by ion-beam thinning of crystals removed from petrographic thin sections, using copper discs for support. Observations were all made using a JEOL JEM 100CX instrument operating at 100 kV. Kalsilite and nepheline are sensitive to beam damage but survive long enough to yield reasonable bright-field images, dark-field images, and diffraction patterns. Grains from mineral separates used in the heating experiments were also examined. They were mounted in epoxy resin, prepared as thin sections, and then ion-beam thinned, with titanium grids used for support. Preparation for the TEM experiments in this way involved heating the samples to ~130 °C for ~15 min to ~1 h to harden the epoxy and melt the thin-section mounting medium.

### IR spectroscopy

In this study, IR spectra were collected only to make the simplest of "fingerprinting" comparisons between different structure types. Samples were ground into a powder for about 5 min by hand in a mortar and pestle, and

**TABLE 2.** Representative chemical analyses of kalsilite, nepheline, and tetrakalsilite

| | 1 | 2 | 3 | 4 | 5 | 6 | 7 | 8 | 9 |
|---|---|---|---|---|---|---|---|---|---|
| $SiO_2$ | 37.40 | 37.75 | 37.62 | 41.42 | 37.99 | 41.07 | 40.45 | 39.27 | 40.45 |
| $Al_2O_3$ | 30.90 | 31.40 | 31.00 | 33.59 | 31.04 | 33.73 | 33.20 | 31.86 | 32.86 |
| $Fe_2O_3$ | 1.32 | 1.22 | 0.70 | 0.71 | 0.88 | 0.92 | 0.84 | 0.76 | 0.80 |
| $Na_2O$ | 1.43 | 2.33 | 0.90 | 15.06 | 2.04 | 14.41 | 12.69 | 5.15 | 9.87 |
| $K_2O$ | 27.93 | 26.48 | 28.61 | 8.90 | 27.40 | 10.01 | 12.65 | 22.72 | 15.99 |
| Total | 98.98 | 99.18 | 98.83 | 99.68 | 99.35 | 100.14 | 99.83 | 99.76 | 99.97 |
| Si | 1.00 | 1.00 | 1.00 | 1.02 | 1.00 | 1.01 | 1.00 | 1.01 | 1.01 |
| Al | 0.97 | 0.97 | 0.97 | 0.97 | 0.97 | 0.97 | 0.97 | 0.97 | 0.97 |
| $Fe^{3+}$ | 0.03 | 0.02 | 0.01 | 0.01 | 0.02 | 0.02 | 0.02 | 0.01 | 0.01 |
| Na | 0.07 | 0.12 | 0.05 | 0.72 | 0.11 | 0.68 | 0.61 | 0.26 | 0.48 |
| K | 0.95 | 0.89 | 0.97 | 0.28 | 0.92 | 0.31 | 0.40 | 0.75 | 0.51 |
| Total | 3.02 | 3.00 | 3.00 | 3.00 | 3.02 | 2.99 | 3.00 | 3.00 | 2.98 |

*Note:* 1 = Kalsilite matrix of Ks-Ne intergrowth; Alban Hills. 2 = Kalsilite; Alban Hills, after homogenization by annealing for 1 d at 950 °C. 3 = Kalsilite (90049). 4 = Nepheline in patches within kalsilite (90049). 5 = Kalsilite (75422). 6 = Nepheline lamellae in kalsilite (75422). 7 = Nepheline overgrowth on a kalsilite phenocryst (75422). 8 = Tetrakalsilite obtained after annealing crystals with Ks-Ne intergrowths from sample 75422 for 1 d at 950 °C. 9 = Nepheline in fine lamellae within the tetrakalsilite of analysis 8. Data collected with a Cameca SX50 electron microprobe using a wavelength-dispersive system for Na and an energy-dispersive system for Si, Al, Cr, Fe, Ti, Mg, K, and Ca (20 kV, 10 nA). Only Si, Al, Fe, Na, and K were detected at levels $>1\ \sigma$ of counting statistics. All Fe was assumed to be $Fe^{3+}$. Oxide values in weight percent.

absorption experiments were performed using the standard pellet technique. The powders were diluted with KBr in the ratio 1:300 for the far infrared region (250–700 $cm^{-1}$) and 1:400 for the middle infrared region (500–1450 $cm^{-1}$). Spectra were collected under vacuum using a Fourier-transformation infrared spectrometer (Bruker IFS 113v). A liquid-nitrogen–cooled MCT detector was used for middle infrared and a room-temperature DTGS detector for the far infrared. The spectral resolution was set to 2 $cm^{-1}$ for middle infrared and to 4 $cm^{-1}$ for far infrared. The zero filling factor for the Fourier-transform algorithm was 4 because final spectral resolutions of 0.5 and 1 $cm^{-1}$, respectively, were obtained. For each sample the spectra in the far and middle region were normalized with respect to the maximum point of the 690 $cm^{-1}$ mode and to the minimum point between 500 and 600 $cm^{-1}$.

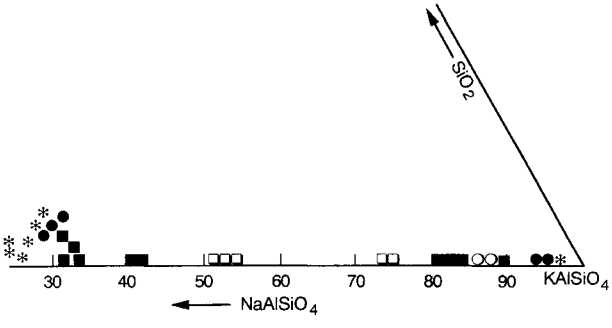


**FIGURE 1.** Compositions of kalsilite, nepheline, and tetrakalsilite (the latter is at ~25% $NaAlSiO_4$). Circles represent samples from Alban Hills; open = homogenized at 950 °C for 1 d, solid = unannealed. Squares represent samples from Mount Nyiragongo, no. 75422; open = homogenized at 950 °C for 1 d, solid = unannealed. Asterisks represent unannealed samples from Mount Nyiragongo, no. 90049; only one composition is shown for the kalsilite in this sample because the analyses obtained were indistinguishable from each other.

## SAMPLE DESCRIPTION

### Starting materials

Metamorphic kalsilite was separated from two samples of a granulite facies gneiss from the Punalur district in Kerala, southern India. The first was that used by Capobianco and Carpenter (1989), which was kindly provided by M. Sandiford (University of Adelaide, Australia), and the second was kindly provided by M. Santosh (Centre for Earth Science Studies, Akkalum, Trivandrum, India). This kalsilite is essentially end-member $KAlSiO_4$, with only ~0.002 $Na^+$ ions per $K^+$ ion and an equivalent proportion of Fe substituted for Al (Capobianco and Carpenter 1989; Sandiford and Santosh 1991). Peak metamorphic conditions for the Punalur assemblages (kalsilite, leucite, hibonite, spinel, corundum, sphene, perovskite, Ti-bearing phlogopite, and potassium feldspar) have been estimated to be 700–800 °C and 3.5–6.5 kbar (Sandiford and Santosh 1991).

Volcanic kalsilite was separated from an ejected block of the "welded scoriae" formation of Colle Cimino (Marino), Alban Hills, Italy, which was kindly provided by A. Cundari (University of Melbourne, Australia). A description of these blocks, and the nepheline-kalsilite microperthites within them, was given by Federico (1976) and Aurisicchio and Federico (1985). Both kalsilite and kaliophilite have been found in the ejecta but not in coexistence. This suggests different crystallization histories for the two phases, perhaps because of variations in chemistry, temperature, or pressure in their respective environments of formation. In thin section the rock from which the kalsilite was separated consisted mainly of diopside and kalsilite; the latter contained ~10% nepheline lamellae exsolved on an optical scale. Powder X-ray diffraction of the kalsilite separate, using a Huber 621 Guinier camera with Cu$K\alpha_1$ radiation, confirmed that kalsilite was the predominant phase, with only a few weak reflections from nepheline. A typical composition of the

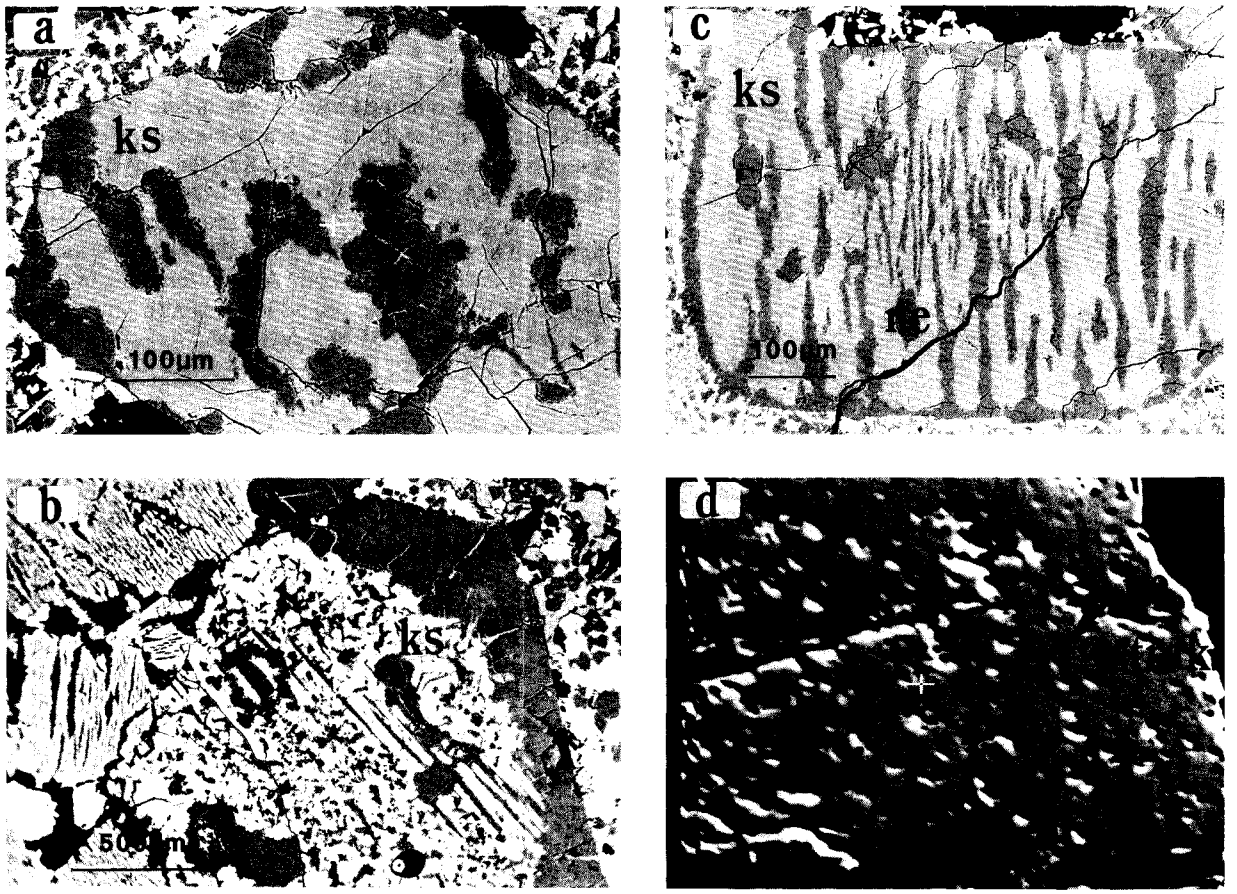


FIGURE 2. SEM images (backscattered electrons) showing phenocrysts of intergrown kalsilite (ks) and nepheline (ne) from Mount Nyiragongo (**a–c**). (**d**) Tetrakalsilite (tetrak) intergrown with fine lamellae of nepheline (ne) after annealing crystals from the same sample as shown in **a–c** at 950 °C for 1 d and quenching in water.

host kalsilite was determined by electron microprobe analysis to be $Ne_7Ks_{93}$ (Table 2, Fig. 1). No significant compositional variations within individual grains or between grains were detected.

Nepheline-kalsilite phenocrysts were selected from porphyritic lavas of the Virunga volcanic field in North Kivu, Mount Nyiragongo, Zaire (sample nos. 75422 and 90049, Harker collection, University of Cambridge). Similar material has been described in detail by Sahama (1957, 1960, 1962). As illustrated in Figure 2, these phenocrysts display a variety of intergrowth textures; some consist of perthitic kalsilite with nepheline lamellae, whereas in others the nepheline occurs as patches in the kalsilite (see Sahama 1960, 1962). The intergrown regions are surrounded by a homogeneous nepheline rim, which has a higher K content than the nepheline lamellae. Compositional data for these samples are given in Table 2 and Figure 1. Sahama (1957) and Smith and Sahama (1957) reported the presence of trikalsilite in the nepheline-kalsilite perthites, but this phase was not found during the course of the present study.

## Annealed samples

Annealing experiments were performed on the Alban Hills and Mount Nyiragongo samples in an attempt to produce homogeneous crystals. The separated powders were wrapped in platinum foil and supported in conventional vertical resistance furnaces. Kalsilite samples with fine nepheline lamellae from the Alban Hills were annealed for 1 d at 950 °C and then quenched in water. The annealed product consisted only of kalsilite, as shown by the disappearance of the nepheline reflections in powder diffraction patterns. The change in lattice parameters is also consistent with homogenization ($a$ = 5.160 and $c$ = 8.683 Å before annealing, $a$ = 5.151 and $c$ = 8.655 Å after annealing). (The $c$ parameter, in particular, is sensitive to composition, e.g., Fig. 3 of Hovis et al. 1992). The average composition of homogenized crystals, from probe analyses, is $\sim Ne_{12}Ks_{88}$ (Table 2, Fig. 1).

Crystals from Mount Nyiragongo (sample no. 75422) were annealed for 1 d at 950 °C and then quenched in water. The product crystals still contained some lamellar

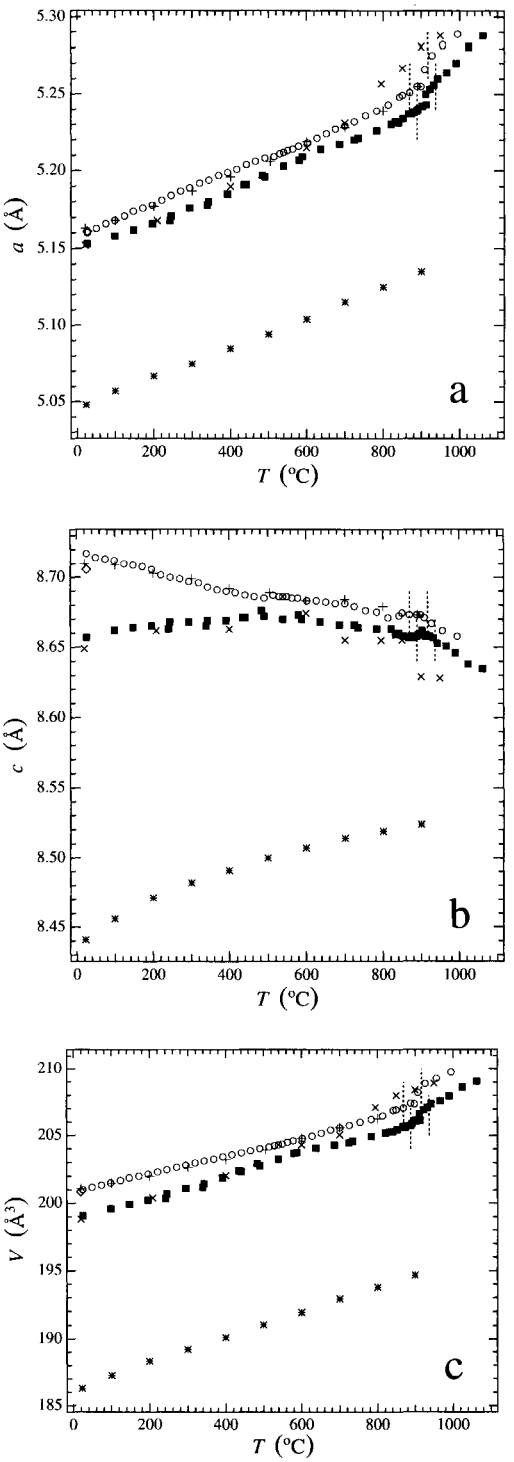


FIGURE 3. (a–c) Thermal expansion behavior on heating of metamorphic kalsilite $Ks_{100}$ (open circles) and homogenized $Ks_{88}$ from Alban Hills (solid squares). A diamond represents $Ks_{100}$ after cooling from high $T$. The other data are from the literature for comparison: plus signs = synthetic kalsilite (Henderson and Taylor 1988); Xs = synthetic kalsilite (Kawahara et al. 1987); asterisks = natural nepheline from Nyiragongo (Sahama 1962), plotted as if it has the same unit cell as kalsilite. Vertical dashed lines indicate the limits of the two-phase intervals.

patches of nepheline (Fig. 2d), but powder X-ray diffraction revealed that the dominant phase had transformed to tetrakalsilite, as found by Sahama (1957). The same products were obtained after annealing for 13 d using a different grain size for the starting material. Probe analysis gave compositions of $\sim Ne_{26}Ks_{74}$ for the tetrakalsilite and $\sim Ne_{48}Ks_{52}$ for the nepheline lamellae (Table 2, Fig. 1).

Small quantities of the $Ks_{100}$ metamorphic kalsilite were annealed in platinum envelopes at 500 (1 h, 4 d) and 950 °C (1 d) and quenched in air. A small amount of Ne-Ks separated from sample no. 90049 was also annealed for 1 d at 950 °C for TEM observations.

## RESULTS

### Powder X-ray diffraction

Refined lattice parameters for the metamorphic kalsilite ($\sim Ks_{100}$) and homogenized Alban Hills kalsilite ($\sim Ne_{12}Ks_{88}$) are shown as a function of temperature in Figure 3. The data for $Ks_{100}$ were collected using two batches of the sample used by Capobianco and Carpenter (1989). The first experiment was from room temperature to ~850 °C, and the second from ~850 to ~1000 °C. Data for $Ks_{88}$ were also collected in two batches, the first from room temperature to ~900 °C, and the second from room temperature to ~1060 °C. Published data for two synthetic kalsilite samples (Henderson and Taylor 1988; Kawahara et al. 1987) and natural nepheline (Sahama 1962) are included for comparison. The $a$ parameter of the $Ks_{100}$ and $Ks_{88}$ samples increased approximately linearly up to ~900 °C, where a discontinuity and an abrupt change in slope occur (Fig. 3a). The $c$ parameter of $Ks_{100}$ decreased approximately linearly, with a break in slope at about the same temperature as for the $a$ parameter. In $Ks_{88}$, the $c$ parameter at first increased but then decreased with increasing temperature (Fig. 3b). The volume expansion (Fig. 3c) is dominated by the contribution from the variation in $a$ for both samples. There also appears to be a change in the trends of $a$, $c$, and $V$ at ~500 °C, which is most evident in the variation of $c$ for $Ks_{88}$ and of $V$ for $Ks_{100}$. The synthetic kalsilite of Henderson and Taylor (1988) is almost indistinguishable from natural $Ks_{100}$ in its thermal evolution, whereas the synthetic sample of Kawahara et al. (1987) behaved more like $Ks_{88}$.

Powder patterns from $Ks_{88}$ obtained at temperatures between ~480 and ~770 °C contained nepheline reflections, showing that exsolution had occurred within the time scale of the data collection. Tuttle and Smith (1958) described similar in situ effects, with the onset of exsolution occurring at 450–500 °C on the nepheline side of the Ne-Ks solvus. In the present experiments the nepheline reflections disappeared above ~770 °C, showing that the sample had rehomogenized. This unmixing might account for the nonlinearity in $a$ and $V$ over the same temperature interval (Figs. 3a and 3c) but cannot be responsible for the nonlinearity in $c$ over the full temperature range.

Three types of structural changes are also indicated by the intensities of the $hhl$, $l$ = odd reflections in the powder

patterns. First, the intensities of these reflections were low in patterns from the metamorphic $Ks_{100}$ sample at room temperature but increased irreversibly between ~250 and ~350 °C during heating (see also Capobianco and Carpenter 1989). Second, there was a transition regime, between ~870 and 920 °C in the present study, characterized by the appearance of superstructure reflections, decreasing intensity of *hhl*, $l$ = odd lines and splitting of lines with large values of $h$ and $k$ relative to $l$. The superstructure reflections faded above ~920 °C. Capobianco and Carpenter (1989) used a quite different experimental set up and obtained 860–920 °C for the transition interval. Andou and Kawahara (1982) and Kawahara et al. (1987) reported that the intensities of *hhl*, $l$ = odd reflections diminished drastically at ~865 °C and were absent above ~875 °C, but they did not comment on the extra reflections that can be seen in their published powder patterns (see discussion in Capobianco and Carpenter 1989). Henderson and Taylor (1988) gave 890 °C for the onset temperature of structural changes, and Sandomirskiy and Urusov (1988) found what appears to be the same transition at 870 ± 20 °C. Third, on quenching the $Ks_{100}$ sample back to room temperature from ~1000 °C, the $c$ parameter consistently decreased from the starting value of 8.717(1) to 8.706(1) Å, with $a$ unchanged. Capobianco and Carpenter associated this effect with possible volatilization of K, but no evidence of leucite formation, which would indicate alkali loss, was found in the present investigation.

No change in the intensity of *hhl*, $l$ = odd reflections was found at low temperatures for the $Ks_{88}$ sample, but a high-temperature transition region was again found. At ~890 °C a few weak superstructure reflections appeared and could be indexed on the basis of the tetrakalsilite structure, with $a = 4A$ and $c = C$. The *hhl*, $l$ = odd reflections weakened from ~890 °C until they disappeared between ~930 and 940 °C, suggesting a change of symmetry from $P6_3$ to $P6_3mc$. For consistency with the description of kalsilite, this $P6_3mc$ structure is referred to in the present study as high tetrakalsilite. The transition region is interpreted as the coexistence interval of low kalsilite and high tetrakalsilite. Reflections with large values of $h$ and $k$ relative to $l$ were broad or showed clear splitting. For example, the 110 reflections of kalsilite decreased in intensity with increasing temperature in this range and were replaced by the 440 reflection of tetrakalsilite at lower $2\theta$. The cell parameters of the two phases remained distinct, and the proportion of high tetrakalsilite appeared to increase with increasing temperature. The powder patterns collected from ~940 to ~1060 °C could all be indexed as high tetrakalsilite. On quenching back to room temperature the $a$ and $c$ parameters could not be distinguished as consistently from their starting values as in the case of $Ks_{100}$ (Table 1). For both $Ks_{100}$ and $Ks_{88}$ the transition range can be accounted for by a first-order transition, with high- and low-temperature phases coexisting isochemically. In each case the high-temperature phase, with presumed $P6_3mc$ symmetry, reverted to a low-temperature $P6_3$ form on cooling.

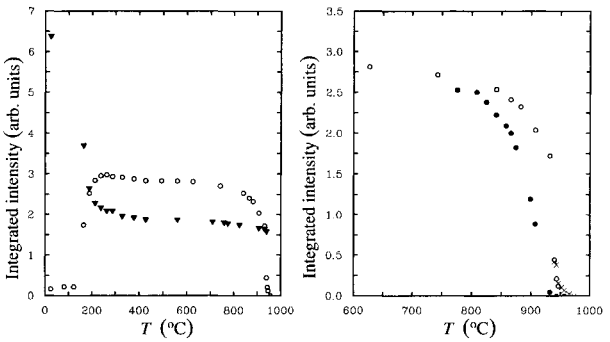


**FIGURE 4.** (**left**) Integrated intensities of the 111 (open circles) and 112 (solid triangles) reflections during heating of $Ks_{100}$. (**right**) Integrated intensities of 111 on heating (open circles) and cooling (solid circles). The intensity of the superstructure reflection 650 (indexing for this reflection based on 660 of the superstructure = 110 of the 1$A$ structure) was measured during a heating cycle (Xs) but only above ~945 °C. The intensity loss of 112 and gain of 111 on heating to ~350 °C was irreversible.

Lattice parameter data were not collected for Mount Nyiragongo kalsilite because fully homogeneous crystals were not obtained. Instead, the development of tetrakalsilite in crystals from sample no. 90049 was followed during in situ heating experiments. Diffraction patterns were collected in steps of ~100 °C from ~580 to ~870 °C. At ~870 °C the *hhl*, $l$ = odd reflections of kalsilite became weak, indicating the onset of a transition from the low to the high structural state. After ~1 h at ~870 °C, tetrakalsilite reflections could be detected. The spectra still contained weak nepheline peaks, showing incomplete homogenization. After cooling to room temperature at 10°/min, the high-temperature pattern remained essentially unchanged except that *hhl*, $l$ = odd reflections reappeared. The final product was therefore an intergrowth of nepheline and low tetrakalsilite. These in situ experiments match the results of the anneal and quench experiments on similar samples reported by Sahama (1957). He produced tetrakalsilite by annealing at temperatures above ~855 °C; annealing at 885–1000 °C, followed by quenching, produced mixtures of tetrakalsilite, nepheline, and kalsilite.

### Single-crystal diffraction

The 111 and 112 reflections (and their symmetry equivalents) were selected for systematic study. If a symmetry change from $P6_3$ to $P6_3mc$ occurs, all reflections with *hhl*, $l$ = odd become extinct; therefore, 111 is a marker for the transition. The only influence of temperature on the 112 substructure reflection should be a steady decrease in intensity with increasing temperature because of normal thermal motions. Because 111 and 112 have similar $(\sin\theta)/\lambda$, the intensity variations of 112 ($I_{112}$) should provide a measure of the contribution of the Debye-Waller factor to the intensity variation of 111 ($I_{111}$). Superstructure reflections within the $a^*$-$b^*$ plane were examined to follow the development and evolution of 4$A$ and 6$A$ superstructures.

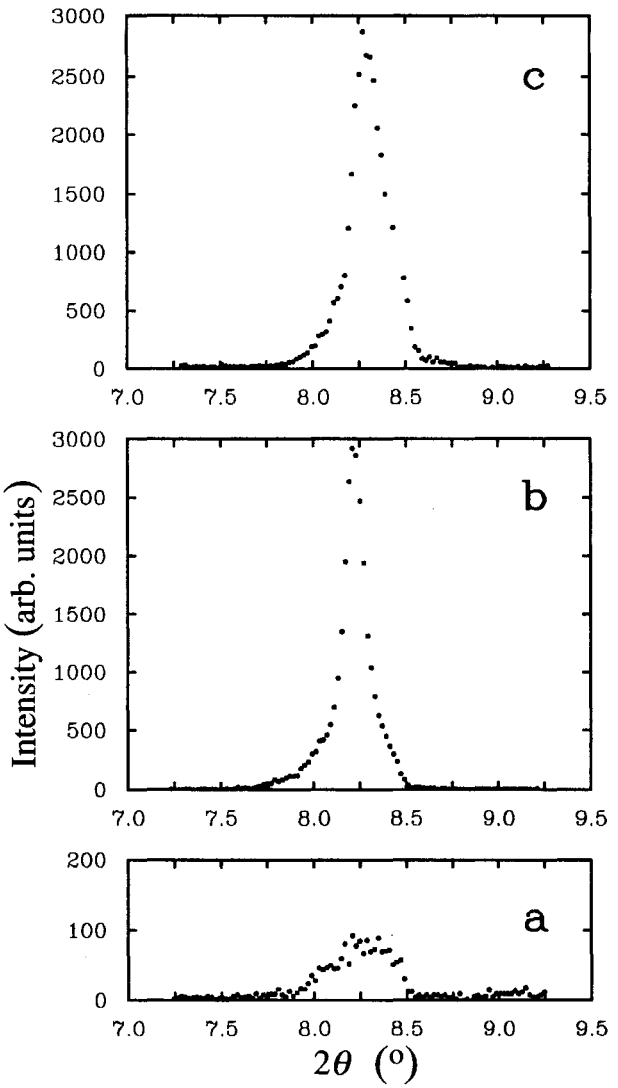


FIGURE 5. Intensity profiles of the 111 reflection for $Ks_{100}$ at (**a**) room temperature before the heating experiment, (**b**) 500 °C, and (**c**) room temperature after the heating experiment. In **b** and **c** a relatively sharp reflection appears to be superimposed on a broader reflection similar to that of the starting material shown in **a**.

In $Ks_{100}$ (the second sample, provided by M. Santosh), the 111 reflection was weak at room temperature but became more intense on heating to ~150 °C (Fig. 4). In the powdered samples the same change was observed at somewhat higher temperatures. The accompanying reduction in $I_{112}$ shows that significant structural changes must have occurred during this irreversible process. The peak profile of 111 illustrated in Figure 5 shows an initially weak and broad reflection, which became sharp at higher temperature and remained relatively intense but slightly broader on quenching from ~1000 °C. Some of the intensity from the initial broad peak appears to have persisted through the heat treatment and is evident on the low $2\theta$ side (Fig. 5).

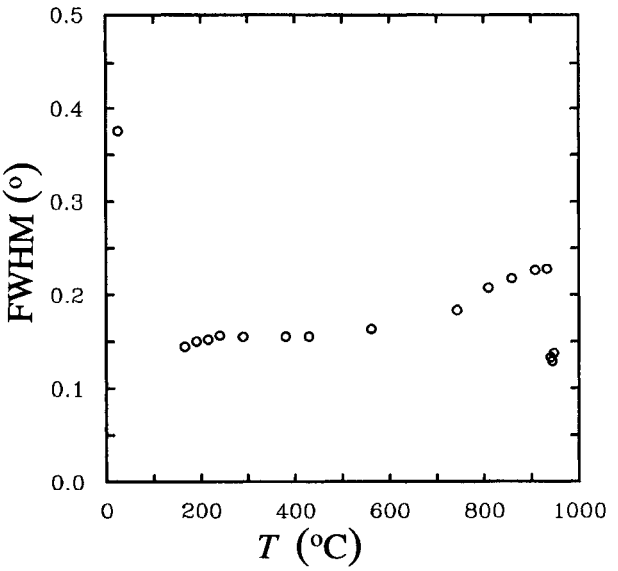


FIGURE 6. Peak width at half-maximum height for the 111 reflection of $Ks_{100}$.

$I_{111}$ dropped off precipitously between ~850 and ~950 °C (Fig. 4), corresponding closely to the transition range observed by powder diffraction. Only relatively minor variations in the peak width were observed, though there is an apparent step at the highest temperatures when $I_{111}$ becomes very small (Fig. 6). The intensity returned on cooling but with a hysteresis of ~50 °C (Fig. 4). The only superstructure reflections found in the $a^*$-$b^*$ plane were those of the $6A$ superstructure. One such reflection, indexed as 650 for the superstructure (660, superstructure = 110, $1A$ structure), was followed above 945 °C in the heating cycle to find the upper stability limit of the superstructure. It tailed off at about the same temperature (~950–960 °C) that $I_{111}$ decreased to zero (Fig. 4), confirming that the high-temperature state ($T >$ ~950 °C) is indeed high kalsilite. These results are consistent with the single crystals having developed a two-phase assemblage, low kalsilite + high ($P6_3mc$) hexakalsilite, in the transition range, though they do not rule out $P6_3$ as the space group of hexakalsilite.

The evolution of $I_{111}$ and $I_{112}$ and the development of superstructure reflections in homogenized $Ks_{88}$ single crystals are illustrated in Figure 7. A steady state must have been achieved quickly at each temperature as no changes in intensity were detected as a function of time. The observed intensities were reproducible over two heating and cooling cycles. Up to ~850 °C, the steady decline of $I_{111}$ and $I_{112}$ is entirely consistent with normal thermal vibrational effects. $I_{111}$ then decreased rapidly but continuously at the same time that $I_{12.10}$, from the $4A$ superstructure, increased. A hysteresis of ~40 °C occurred on subsequent cooling. The 111 reflection was broad from the start and only broadened further at ~900 °C (Fig. 8), when the reflection tailed off to its lowest intensity level. The data are entirely consistent with a

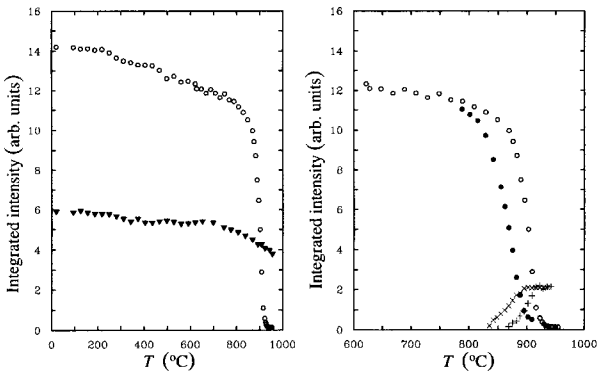


FIGURE 7. (**left**) Integrated intensities of the 111 (open circles) and 112 (solid triangles) reflections during heating of homogenized $Ks_{88}$. (**right**) Integrated intensities of 111 reflection on heating (open circles) and cooling (solid circles), and of the superstructure reflection 12.10 for a cell with $a = 4A$, $c = C$, on heating (plus signs) and cooling (Xs).

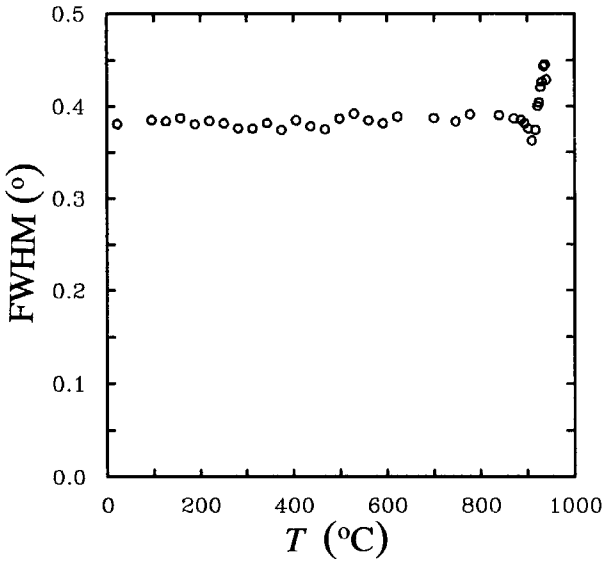


FIGURE 8. Peak width at half-maximum height for the 111 reflection of $Ks_{88}$.

transition region of coexisting $P6_3$ kalsilite and $P6_3mc$ high tetrakalsilite. As temperature increased, the proportion of tetrakalsilite increased until no kalsilite remained.

## TEM observations

**Metamorphic $Ks_{100}$.** New information on the analog phase $KLiSO_4$ (Bhakay-Tamhane et al. 1991; Rajagopal et al. 1991, and references therein) and the failure to find any significant peak splitting in X-ray diffraction patterns that might indicate orthorhombic distortions in pure kalsilite, prompted a thorough reexamination of the metamorphic $Ks_{100}$ sample. TEM observations were made on the second sample, provided by M. Santosh, which, as described by Capobianco and Carpenter (1989) for the sample used for powder diffraction, contained multiple lamellae parallel to (001) on a scale of a few hundred to a few thousand angstroms. Dark-field images using $hhl$, $l$ = odd reflections showed black and white contrast, with a proportion of the lamellae clearly not contributing to reflections that violate the $c$ glide of a $P6_3mc$ structure. The interpretation offered by Capobianco and Carpenter was that only one of the three possible sets of twins of a $Cmc2_1$ structure would have $hhl$, $l$ = odd absent in each $c$*-[110]* section of the reciprocal lattice. An alternative hypothesis is that the lamellae represent an intergrowth of $P6_3$ and $P31c$ structures, sharing (001) and with the same unit cell. This would be consistent with the lack of splitting of $hk0$ reflections if the two phases have the same $a$ dimension and conforms almost exactly to the reported behavior of $P6_3$ $KLiSO_4$ on cooling below room temperature (Bhakay-Tamhane et al. 1991, and see discussion below).

To test the suggestion of a two-phase intergrowth, systematic dark-field experiments were conducted on ion-beam–thinned specimens, and the observed intensity distributions were compared with X-ray structure factors, $F_{hkl}$, for the two structures. $F_{hkl}$ values were calculated for $P6_3$ kalsilite using the refined atomic coordinates given by Andou and Kawahara (1984). A hypothetical $P31c$ kalsilite structure was created by analogy with $KLiSO_4$, in which the atomic positions are almost identical in the asymmetric units of both $P6_3$ and $P31c$ phases (Bhakay-Tamhane et al. 1991). The $P6_3$ coordinates of Andou and Kawahara (1984) were taken directly to represent the asymmetric unit in the structure-factor calculations for $P31c$ kalsilite. Two types of merohedral twinning can occur (Bhakay-Tamhane et al. 1991). $P6_3$ (Laue class $6/m$) twins are related to each other by reflection across a plane parallel to the $c$ axis such that the diffraction pattern from an area of crystal containing both twins has the $hkl$ reflection from twin 1 superimposed on the $khl$ reflection from twin 2 (and $khl$ from twin 1 superimposed on $hkl$ from twin 2). Because structure factors $F_{hkl}$ and $F_{khl}$ are not identical under $P6_3$ symmetry, the dark-field image obtained using a superimposed $hkl$ (twin 1) and $khl$ (twin 2) reflection should show the twins in contrast. Equivalently for the $P31c$ structure (Laue class $\bar{3}m$), $F_{hkl}$ is not related by symmetry to $F_{hkl}$, and the $hkl$ reflection from twin 1 is superimposed on the $hk\bar{l}$ reflection of twin 2 ($hk\bar{l}$ of twin 1 is likewise superimposed on $hkl$ of twin 2). Dark-field images using a reflection of this form should therefore show the $P31c$ twins in contrast. These critical structure-factor relationships are evident in the selected values given in Table 3.

Figure 9 contains a $c$*-[110]* section imaged with 111 (Fig. 9a) and 112 (Fig. 9b) reflections. The contrast between the two images is reversed: The darkest lamellae in one image are the lightest in the other. This is at least consistent with the calculated X-ray structure factors because there should be no intensity contribution to 111 from $P31c$ lamellae, and $I_{112}$ is expected to be greater from $P31c$ than $P6_3$ structures (Table 3). Two areas of

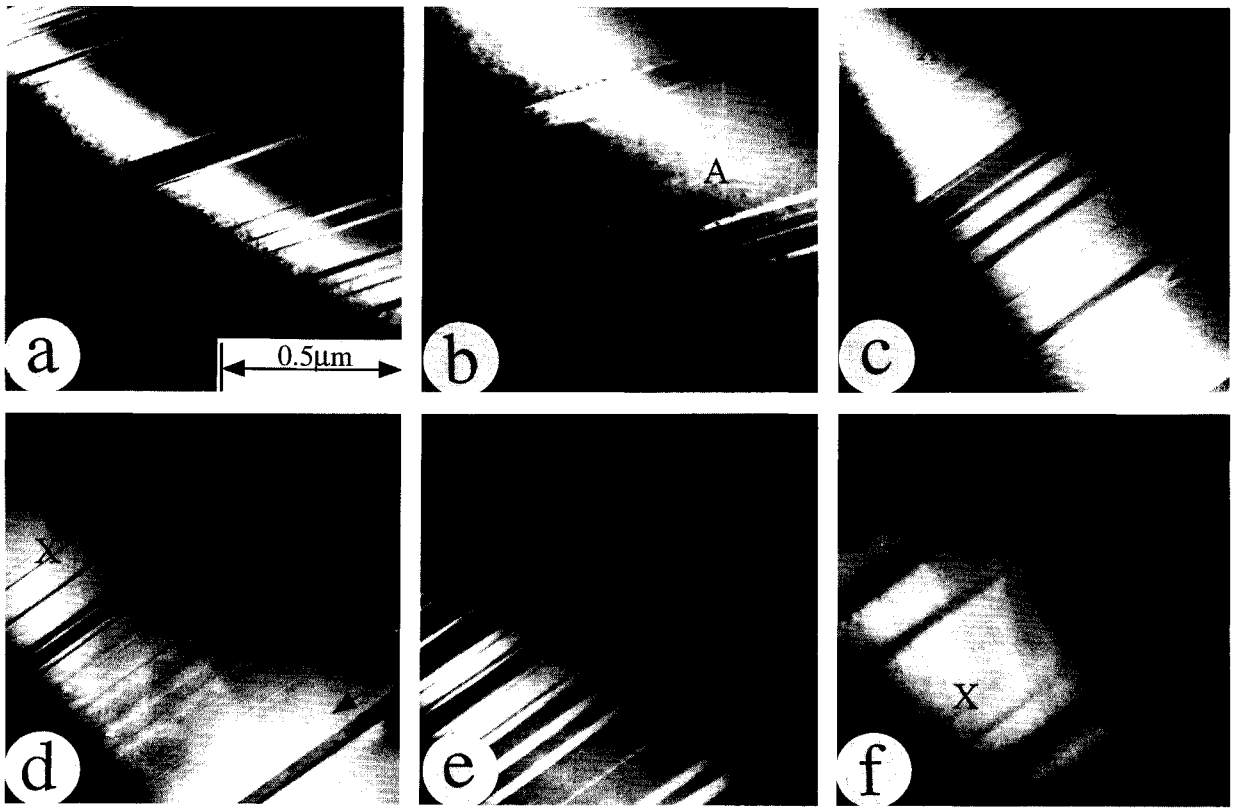


**FIGURE 9.** Dark-field electron micrographs of metamorphic $Ks_{100}$ (all at the same scale). (**a**) Section approximately parallel to $c^*$-[110]*, **g** = 111. Dark lamellae parallel to (001) are interpreted as having $P31c$ symmetry. (**b**) Same area as **a**, **g** = 112. Lamellae interpreted as having the $P31c$ structure in **a** are lightest (largest intensity contribution to 112), as expected from calculated $F_{hkl}$ values (Table 3). Very weak contrast from $P6_3$ twins (e.g., the twin labeled A) is assumed to be anomalous and due to the fact that ideal two-beam conditions were not obtained. A characteristic pattern of beam damage is the development of relatively ragged twin boundaries, as most clearly seen at the topmost boundary. (**c**) Section approximately parallel to $c^*$-[210]*, **g** = 211. The (001) lamellae show three shades of contrast. (**d**) Same area as **c**, **g** = $21\bar{1}$. The lamellae indicated by arrows now show reverse contrast with respect to **c** and must correspond to the two possible $P31c$ twins. (**e**) Same area as **c** and **d**, **g** = 210. The lightest areas (greatest diffraction contribution to 210) have $P31c$ symmetry on the basis of the calculated structure factors. (**f**) Same area as **c**, **d**, and **e**, **g** = $\bar{1}\bar{1}3$. The light areas have $P6_3$ symmetry, and the dark areas have $P31c$ symmetry. An X indicates the same position on the sample in each micrograph.

**TABLE 3.** Calculated structure factors (X-ray scattering) for selected diffraction maxima from $P6_3$ and $P31c$ forms of kalsilite, $KAlSiO_4$

| $hkl$ | $F_{hkl}$, $P6_3$ | $F_{hkl}$, $P31c$ |
|---|---|---|
| 111 | 23.5 | absent |
| 113 | 18.9 | absent |
| 115 | 13.3 | absent |
| 112 | 21.0 | 32.6 |
| $11\bar{2}$ | 21.0 | 27.9 |
| 121 | 17.9 | 15.9 |
| 211 | 17.1 | 15.9 |
| $12\bar{1}$ | 17.9 | 14.2 |
| $21\bar{1}$ | 17.1 | 14.2 |
| 210 | 0.6 | 9.5 |
| 120 | 1.5 | 9.5 |
| 310 | 5.2 | 10.4 |
| 130 | 5.5 | 10.4 |
| 311 | 13.2 | 11.4 |
| 131 | 15.6 | 11.4 |
| $31\bar{1}$ | 13.2 | 11.3 |
| $13\bar{1}$ | 15.6 | 11.3 |

this section (e.g., at A in Fig. 9b) show fine lineations in the 111 image but only the faintest contrast in the 112 image. They are interpreted as containing twins of the $P6_3$ structure; the twin boundaries are in contrast for 111 but out of contrast for 112. The images can be explained, therefore, as containing the two $P6_3$ twins intergrown with $P31c$ lamellae. Exactly the same reversal of contrast was observed using 113 and 114 reflections in a different crystal.

Figure 9 contains images of another area obtained with 211 (Fig. 9c), $21\bar{1}$ (Fig. 9d), 210 (Fig. 9e), and $\bar{1}\bar{1}3$ (Fig. 9f) reflections. The section was approximately parallel to $c^*$-[210]*. The $\bar{1}\bar{1}3$ image is diffuse, partly because of imperfect focusing but also as a consequence of progressive beam damage. From the structure-factor calculations it was anticipated that $I_{210}$ might be much greater for the $P31c$ structure than for the $P6_3$ structure. Thus, the la-

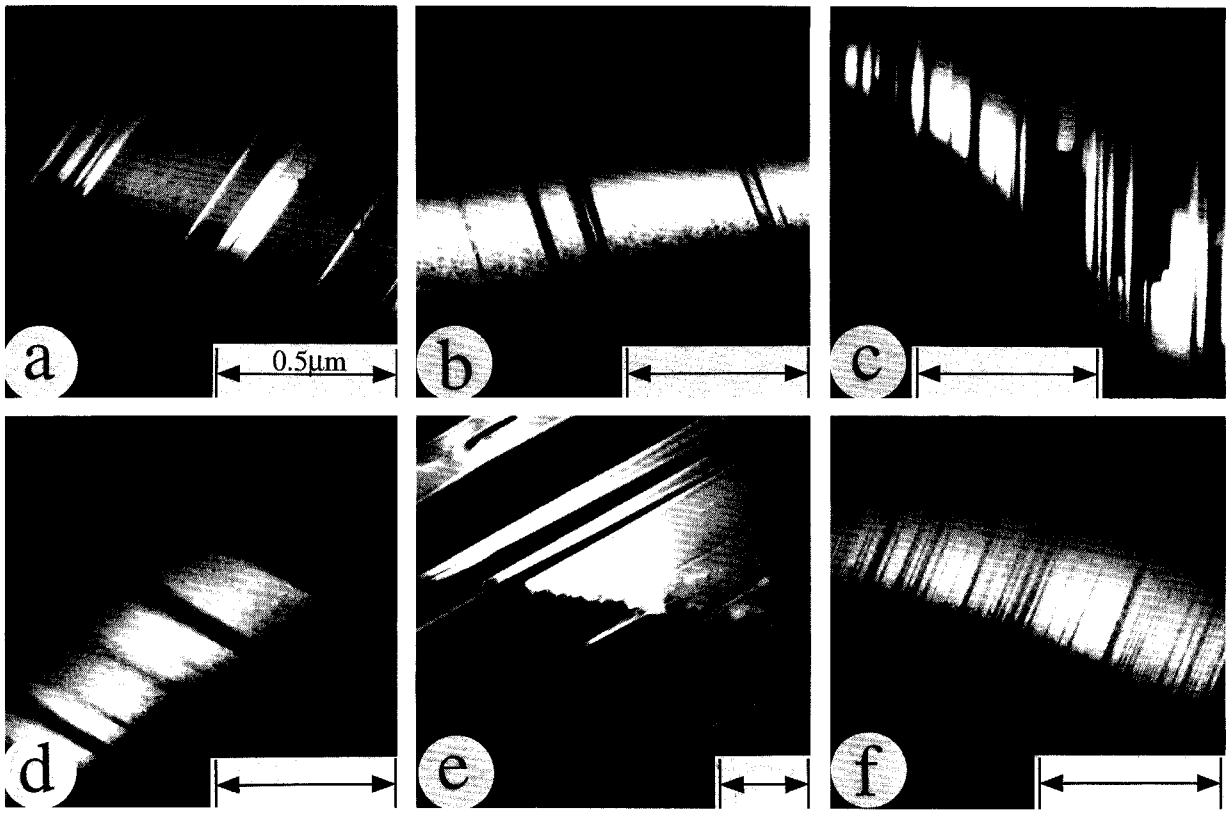


**FIGURE 10.** Variability of (001) lamellar textures in $Ks_{100}$. **(a)** Section approximately parallel to $c^*$-[310]*, **g** = 310. The light lamellae are interpreted as having $P31c$ symmetry, and boundaries between $P6_3$ twins can also be seen (arrows). **(b)** **g** = 111. Predominantly $P6_3$, with (001) twin boundaries and thin $P31c$ lamellae. **(c)** **g** = 113. Larger proportion of $P31c$ than in **b**. The blocky texture could be interpreted as evidence for a ledge mechanism for growth of one phase from the other. **(d)** **g** = 210. ~80% $P31c$. **(e)** **g** = $22\bar{1}$. A ragged interface crosses the (001) lamellae, separating regions of predominantly $P6_3$ material (light) from $P31c$ material (dark). **(f)** **g** = 211. Lamellar spacings are so fine as to resemble (001) stacking faults and could account for the broadening of the 111 reflection shown in Figure 5a.

mellae contributing strongly to the 210 reflection in Figure 9e are interpreted as having the $P31c$ structure. This is confirmed by the $\bar{1}\bar{1}3$ image (Fig. 9f), which has the same lamellae totally out of contrast. In the 211 image (Fig. 9c), the lamellae show two shades of contrast (e.g., arrows). One clearly contributed less intensity to the 211 reflection, whereas the other contributed about the same intensity as the matrix $P6_3$ phase. The contrast of these two $P31c$ twins is reversed on imaging with the $21\bar{1}$ reflection (Fig. 9d). This is once again consistent with the calculated structure factors in Table 3. The reversal of contrast between 211 and $21\bar{1}$ dark-field images could not occur if the twin lamellae had a $Cmc2_1$ structure because $F_{211}$ and $F_{21\bar{1}}$ are equivalent by symmetry in Laue class $mmm$. This section is therefore interpreted as containing lamellae with the $P6_3$ structure in one twin orientation intergrown with both of the possible $P31c$ twins.

Figure 10a contains lamellae imaged with the 310 reflection. $F_{hkl}$ calculations indicate that $I_{310}$ could be significantly greater for the $P31c$ structure than for the $P6_3$ structure. Accordingly, the more intensely diffracting lamellae were expected to be $P31c$ kalsilite and to show only one shade of contrast. The less intensely diffracting regions actually contain two sets of lamellae with approximately the same weak contrast, corresponding to the two $P6_3$ twins. Other dark-field images support the same explanation in every case examined in any detail, namely that the $Ks_{100}$ sample contains lamellae of two $P6_3$ twins intergrown with two $P31c$ twins. The proportion of $P6_3$ and $P31c$ phases varied widely even within a single crystal, from being more than ~90% $P6_3$ (Fig. 10b) to ~50:50 (Fig. 10c) to ~80% $P31c$ (Fig. 10d) and more than ~90% $P31c$ (Fig. 10e). In some cases the spacing of the twin lamellae was so fine as to resemble (001) stacking disorder (Fig. 10f). Although the lamellae tended to have parallel boundaries, some showed a characteristic blocky texture (Fig. 10c), such as might arise by ledge growth of one twin from another. In rare instances this was on a coarser scale with a broad stepped interface at a steep angle to (001), illustrated in Figure 10e. One dark-field image from an $a^*$-$b^*$ section showed twin boundaries parallel to {100}. These were presumably the twin bound-

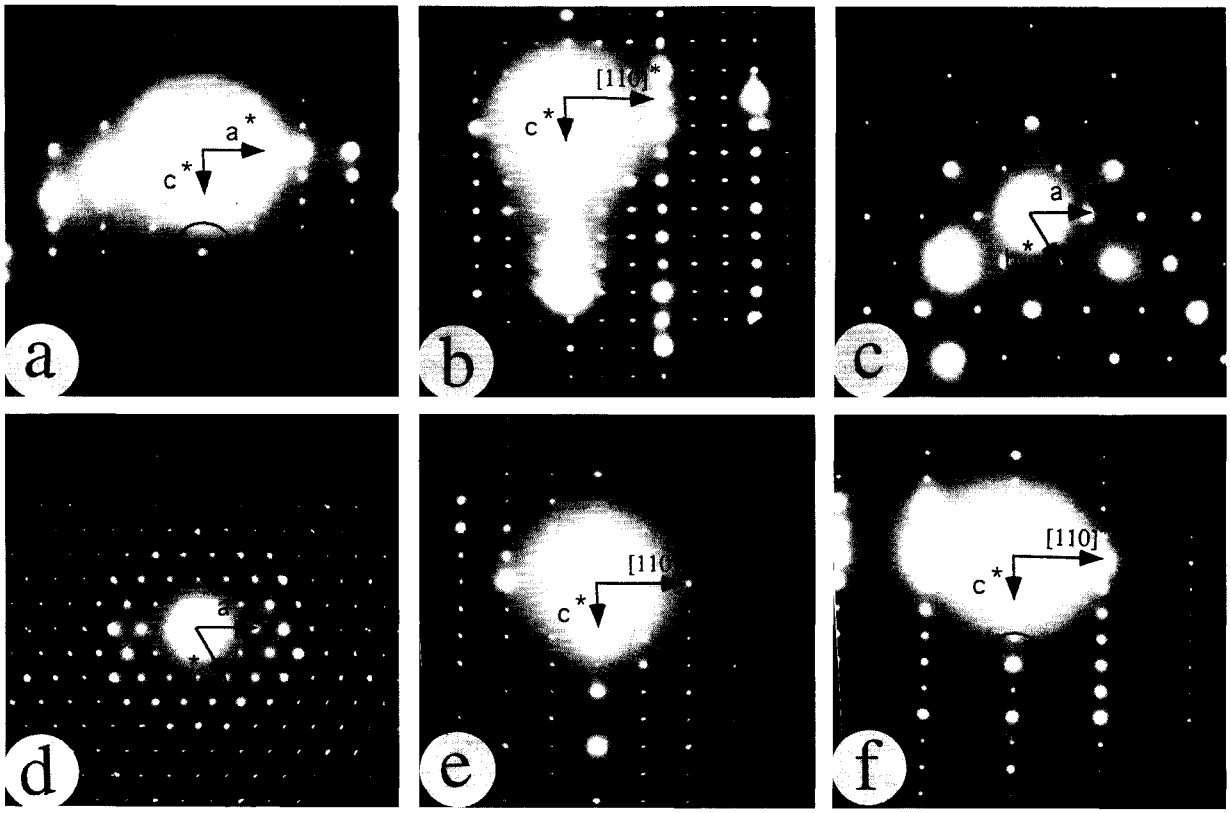


**FIGURE 11.** Selected-area diffraction patterns, overexposed to reveal diffuse intensity. (**a**) $a^*$-$c^*$ section of $Ks_{100}$. Note the curved bands of diffuse intensity passing through many of the reflections. (**b**) $c^*$-[110]*, kalsilite from Mount Nyiragongo, 75422. Superstructure reflections defining tripling parallel to [110]* are diffuse. Some weak, curved diffuse bands similar to those in **a** were more clearly visible on the original photographic plate. (**c**) $a^*$-$b^*$, kalsilite from Mount Nyiragongo, 75422. The $\sqrt{3}A$ superstructure reflections are highly diffuse in this case. (**d**) $a^*$-$b^*$, exsolved nepheline from Alban Hills. The smearing of individual reflections is interpreted as the result of small misorientations between subgrains. (**e**) $c^*$-[110]*, exsolved nepheline from Alban Hills. Doubling along [110]* gives the $2A$ nepheline superstructure, and the curved diffuse intensity (e.g., within ring) is characteristic of volcanic samples (McConnell 1962). In plutonic nepheline, incommensurate reflections replace the diffuse bands. (**f**) $c^*$-[110]*, kalsilite from Alban Hills. The $\sqrt{3}A$ superstructure reflections are highly diffuse; curved diffuse bands are also visible.

aries at steps perpendicular to (001) in sections such as Figure 10c.

Some diffuse intensity was observed in overexposed electron diffraction patterns. This was not fully characterized in three dimensions, but it consisted of curved bands passing through the Bragg reflections in $a^*$-$c^*$ sections (Fig. 11a). It bears some resemblance to the distribution of diffuse intensity in $c^*$-[110]* sections of rapidly cooled natural nepheline crystals described by McConnell (1962) (and see Fig. 11e). Rather similar diffuse scattering was also observed in $c^*$-[110]* sections and included a component parallel to [110]*.

The microstructures in metamorphic $Ks_{100}$ crystals annealed for 1 h at 500 °C consisted of (001) twins on a scale comparable with that of the starting material. Separating the twins were either sharp twin boundaries or narrow lamellae, which were out of contrast in dark-field images formed with $hhl$, $l$ = odd reflections. The latter showed contrast in other dark-field images consistent with their being relict $P31c$ lamellae. Their width was typically less than ~500 Å, though one lamella ~900 Å wide was observed. Crystals annealed for 4 d at 500 °C contained $P6_3$ twins with no detectable $P31c$ lamellae. A reduction in the proportion of the $P31c$ phase at 500 °C is consistent with the powder and single-crystal diffraction data, which showed a steep decrease in $I_{112}$ and a steep increase in $I_{111}$ at temperatures of ~150–350 °C. Crystals annealed for 1 d at 950 °C contained (001) boundaries separating $P6_3$ twins on a scale of several hundreds of angstroms.

Preparation of the crystals for TEM involved heating them to ~130 °C. Given that the single-crystal X-ray study implied that structural changes might occur at a temperature as low as ~150 °C, it is possible that this treatment caused some change to the original microstruc-

ture of the natural sample. The experimental data suggest that any changes, if they did occur, would involve some small reduction in the proportion of the $P31c$ phase present.

**Mount Nyiragongo.** Host kalsilite in the Mount Nyiragongo samples (75422 and 90049) contained twin lamellae parallel to (001), but the average spacing between twin boundaries was at least 5–10 $\mu$m. A small number of narrower twins were found, and these invariably showed the expected dark-field characteristics of $P6_3$ twins. For example, a narrow twin imaged with the 311 reflection and the boundaries of a twin in a different crystal imaged with 113 are shown in Figures 12a and 12b. In some cases the twin boundaries contained 90° steps between straight segments. In the section oriented approximately parallel to $c^*$-[110]* shown in Figure 12c, some of these steps are narrow and sharp, whereas others are broad and contain fringes. The thin boundaries could be parallel to (110), whereas the broader steps are clearly inclined at a steep angle to the section and are not inconsistent with the {100} orientation apparently favored in the metamorphic $Ks_{100}$ sample.

Electron diffraction patterns were indexed as the $\sqrt{3}A$ kalsilite superstructure first reported by Smith and Sahama (1957). Reflections indicating tripling of the unit cell along [110]* were diffuse (Figs. 11b and 11c). Their intensity appeared to vary between different crystals, but they were strong enough, in one case at least, to give a dark-field image containing small antiphase domains (APDs) on a scale of ~100 Å and elongate parallel to $c$ (Fig. 12d). Diffuse intensity was evident both along [110]* and as curved bands emanating from, or passing through, some of the main Bragg peaks in overexposed diffraction patterns. The curved bands were similar to the diffuse bands in pure kalsilite (compare Figs. 11a and 11b).

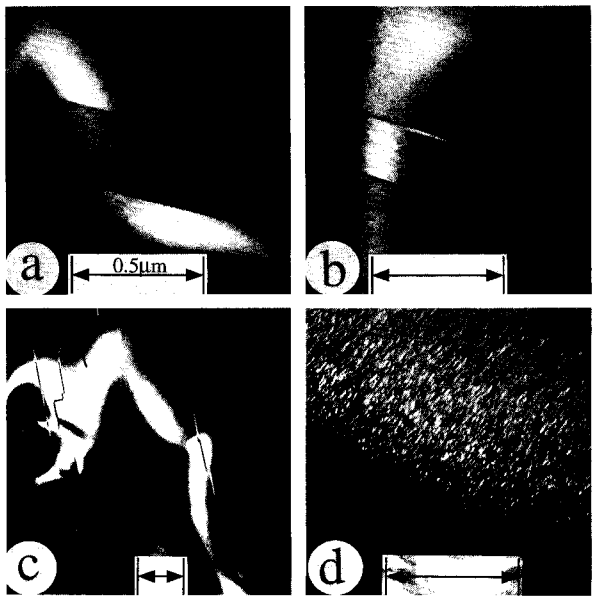


**FIGURE 12.** Microstructures in $P6_3$ kalsilite from Mount Nyiragongo, 75422. (**a**) **g** = 311. Weak contrast between a twin and its host is expected on the basis of the calculated structure factors for 311 and 131 (Table 3). (**b**) **g** = 113. A similar twin to that shown in **a** has contrast only at its boundaries when imaged with an $hhl$, $l$ = odd reflection. (**c**) Section approximately parallel to $c^*$-[210]*, **g** = 113. The long segments of twin boundaries are parallel to (001) and are narrow. Some of the steps between these segments are broad and clearly at a steep angle to the section (e.g., arrow); they could be parallel to (100). (**d**) Imaging with a strong $\sqrt{3}A$ superstructure reflection reveals small APDs, which are slightly elongate parallel to $c$.

Coarse nepheline patches in these crystals, presumably corresponding to the nepheline regions optically visible in thin sections, were readily distinguished from kalsilite in bright-field images by their significantly higher density of dislocations. They also contained twin-domain textures, though with quite different characteristic properties, as illustrated in Figure 13. In $a^*$-$b^*$ sections a distinctive microstructure consisted of criss-crossing twin boundaries parallel to {100} that defined triangular or diamond-shaped twin domains (Fig. 13a). The twin boundaries were not invariably linear, however, and they also showed evidence of interaction with dislocations (Fig. 13b). In sections containing $c^*$, the domain boundaries tended to be aligned approximately parallel to $c^*$, consistent with the {100} orientation inferred from $a^*$-$b^*$ sections (e.g., Fig. 13c). Only one example of a strongly preferred orientation consistent with (001) has been found so far (Fig. 13d). A systematic analysis of the imaging conditions for these domains was not attempted, but contrast was observed in dark-field images using reflections such as 210, 211, 212, 311, and $\bar{2}\bar{1}3$. The domains were out of contrast in dark-field images using 300, 201, and 021 reflections (indexed with respect to the normal $2A$, $P6_3$ nepheline unit cell). The list of X-ray structure factors given for nepheline by Foreman and Peacor (1970) suggests that these contrast conditions are consistent with $P6_3$ twins that might have developed at a $P6_3mc \rightarrow P6_3$ transition. Doubling of the $a$ repeat of nepheline from a parent $1A$ structure could also result in the development of APDs related by displacement vectors $\frac{1}{2}a$, $\frac{1}{2}b$, and $\frac{1}{2}(a + b)$. If they are present, the antiphase boundaries (APBs) should be imaged in dark-field images formed with any reflection having $h$ = odd or $k$ = odd. The microstructure in Figure 13e, imaged with a 211 reflection, contains an irregular, curved boundary transecting two twin boundaries but not influencing the contrast of the domains themselves. A similar looking lineation was observed in another area using 300. These features appeared to be rare and could also be understood as stacking faults generated by the passage of partial dislocations, rather than as transformation-induced APBs.

Exsolution lamellae with widths on a scale of ~1 $\mu$m (Fig. 13c) characteristically had interfaces approximately parallel to (001). There is a substantial volume difference between nepheline and kalsilite, but these lamellae in general showed little evidence of coherency strains; the

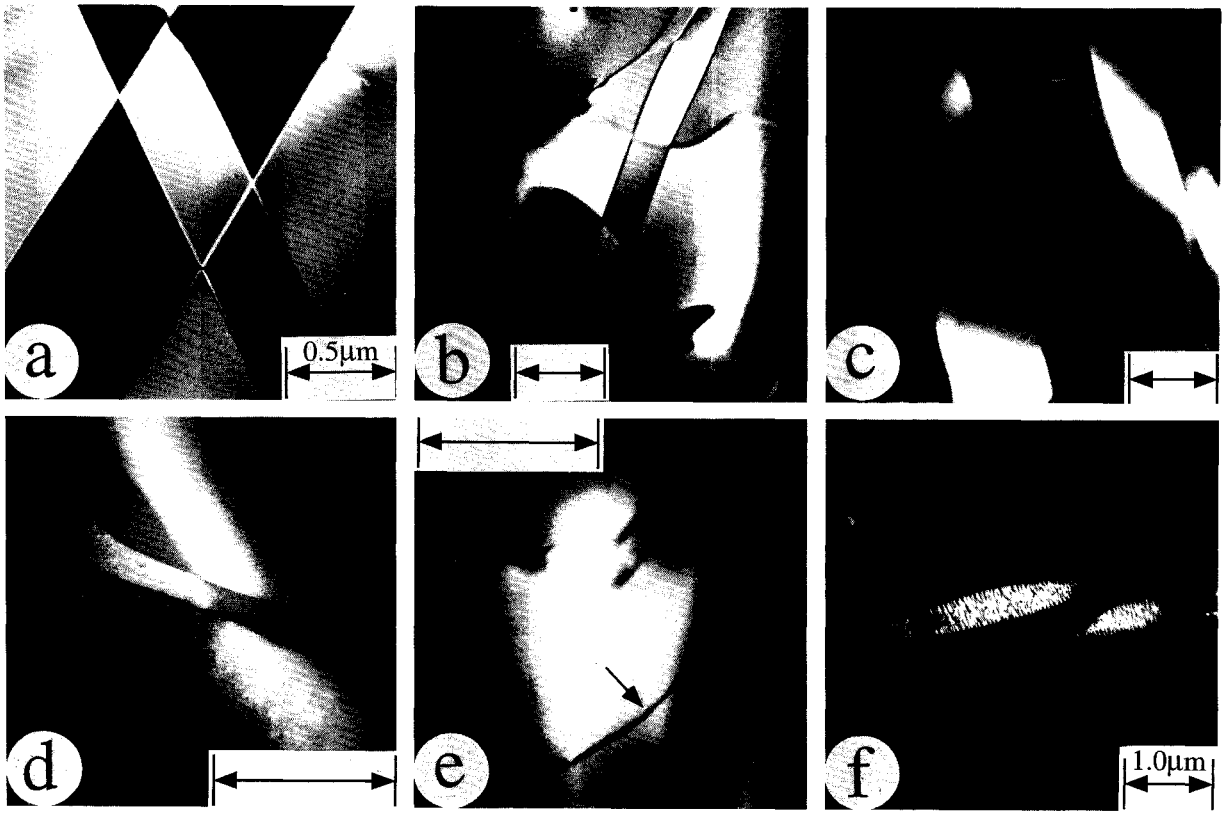


FIGURE 13. Microstructures in nepheline exsolved from Mount Nyiragongo kalsilite. The scale bar indicates 0.5 $\mu$m in **a**–**e**. (**a**) Diamond-shaped twin domains with characteristic boundary orientations approximately parallel to {100} (75422; dark field). (**b**) {100} twin boundaries together with wavy twin boundaries, some of which terminate at or pass through dislocations (90049; bright field). (**c**) Within a single nepheline exsolution lamella, which has ~(001) interfaces with kalsilite, there are twin boundaries approximately parallel to (100) (75422; dark field, **g** = 21*I*Ne). (**d**) ~$c$*-[310]* section showing one straight twin boundary parallel to (001) together with curved boundaries (75422; dark field, **g** = 311Ne). (**e**) Most boundaries observed in dark field clearly separate twin domains. In rare instances, a boundary with no twin contrast was found, such as indicated by an arrow (75422; dark field, **g** = 211Ne). Note that this boundary crosses from one twin domain to another. (**f**) En echelon lozenges of exsolved nepheline in kalsilite, with interfaces generally following a (001) trend. The same type of contrast within the nepheline was observed in bright field and in dark field and is interpreted as indicating strain arising from a more or less coherent interface (75422; **g** = 212Ne).

interfaces are presumed to be incoherent. In the finest scale generation of exsolution, however, small en echelon lozenges of nepheline showed substantial strain contrast, consistent with a more or less regular array of dislocations at the interfaces (Fig. 13f). The interfaces of these lozenges are approximately parallel to (001) but are distinctly curved. Splitting of an original thin lamella into small segments could yield this texture, perhaps in response to a change in orientation of the lowest energy interface between the host kalsilite and exsolved nepheline during cooling.

Nepheline diffraction patterns all conformed to the expected reciprocal lattice of the $2A$, $P6_3$ structure. Overexposed diffraction patterns showed curved diffuse branches of the type reported by McConnell (1962) for volcanic nephelines, illustrated in Figure 11e from the Alban Hills sample. This diffuse intensity is also remarkably similar to that found in the kalsilite patterns (compare Figs. 11a, 11b, 11e).

The tetrakalsilite product of annealing kalsilite-nepheline intergrowths from sample no. 90049 for 1 d at 950 °C gave sharp $4A$ superstructure reflections in electron diffraction patterns. It also contained a domain texture that closely resembled the merohedral twinning microstructure in nepheline from specimen 75422. Tetrakalsilite in the heat-treated sample 75422 had $P6_3mc$ symmetry at 950 °C and $P6_3$ symmetry at room temperature. As argued for nepheline in the Mount Nyiragongo crystals, therefore, twinning in the $4A$ superstructure might have originated at a $P6_3mc \rightarrow P6_3$ transition during cooling.

**Alban Hills.** Twin boundaries were even less frequently observed in the Alban Hills kalsilite than in the Mount Nyiragongo kalsilite. Only one boundary was imaged in

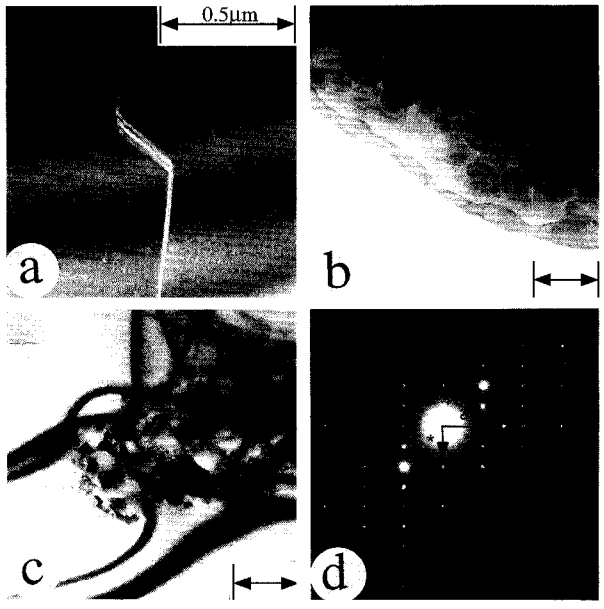


**FIGURE 14.** Microstructures in Alban Hills nepheline and kalsilite. (**a**) Zigzag boundary in kalsilite; segments of the boundary are rotated by ~120° and are consistent in orientation with approximately {100} (dark field, **g** = 011). (**b**) Polygonized texture in exsolved nepheline. Some of the individual subgrains contain straight boundaries consistent with {100} twins (bright field). (**c**) The tip of a thinner lamella of nepheline, which has irregular interfaces with kalsilite and is one subgrain wide (bright field). (**d**) $a^*$-$c^*$ diffraction pattern from kalsilite enclosing a thin nepheline precipitate similar to that shown in **c**. In spite of the Ne-Ks interface being inclined at an angle of ~20° to (001), the two reciprocal lattices share common principal axes.

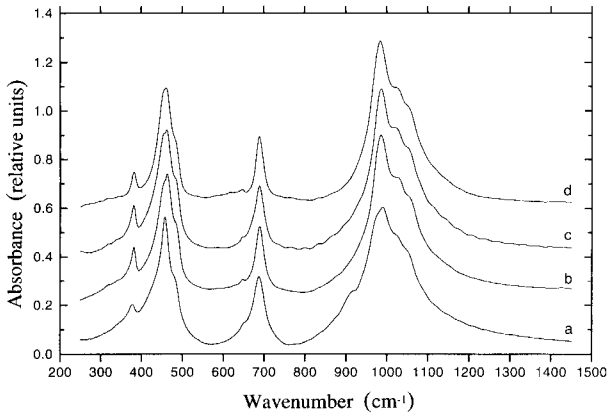


**FIGURE 15.** Infrared spectra at room temperature of (a) homogenized $Ks_{88}$, (b) unannealed $Ks_{100}$, (c) $Ks_{100}$ after annealing at 500 °C for 1 h, and (d) $Ks_{100}$ after annealing at 500 °C for 4 d. In spite of their having different proportions of $P6_3$ and $P31c$ phases, the three $Ks_{100}$ samples have remarkably similar spectra. The $Ks_{88}$ spectrum has additional peaks at ~920 and ~970 $cm^{-1}$.

several crystals, and the domain-wall angles of 120° were consistent with preferred orientations parallel to {100} (Fig. 14a). Nepheline exsolution lamellae consisted of small grains with a fairly uniform dimension of ~0.2 μm (Fig. 14b). These individual grains were slightly misoriented with respect to each other, with a maximum observed misorientation of ~1° (as seen in Fig. 11d) and are assumed to represent subgrains separated by dislocation walls. Within many individual grains, fine lamellae resembling twins were observed, with preferred orientations approximately parallel to {100} (Fig. 14b). Dark-field imaging did not reveal any evidence of a pervasive APD texture, though more or less linear features were occasionally observed. The narrowest exsolution lamellae were only one subgrain (~0.4 μm) wide, with curved or irregular interfaces between host and precipitate (Fig. 14c). No single preferred orientation for the exsolution interfaces was found. Rather, they showed misalignments from (001) varying between ~0 and 50°. A thin nepheline lamella with an interface ~20° from (001) gave a diffraction pattern indicating an almost parallel relationship between the crystallographic axes of the nepheline and kalsilite (Fig. 14d).

Exsolved nepheline in the Alban Hills crystals gave diffraction patterns characteristic of the $2A$, $P6_3$ structure, with the diffuse intensity in curved bands typical of volcanic crystals (Fig. 11e). Diffraction patterns from the host kalsilite were consistent with the $\sqrt{3}A$, $P6_3$ structure, having relatively weak and diffuse $\sqrt{3}A$ superstructure reflections (Fig. 11f). Annealing these crystals for 1 d at 950 °C caused the disappearance of nepheline by rehomogenization but did not markedly alter the apparent structural state of the kalsilite, as discerned from electron diffraction patterns. Only a very small number of $P6_3$ twin boundaries, parallel to (001) and containing jogs approximately consistent with {100}, were found in the annealed crystals.

### IR spectroscopy

The IR spectra of homogenized $Ks_{88}$ crystals, natural $Ks_{100}$, and $Ks_{100}$ after annealing at 500 °C for 1 h and 4 d are shown in Figure 15. The three $Ks_{100}$ samples have different proportions of $P6_3$ and $P31c$ material. After 4 d at 500 °C only the $P6_3$ phase remained, but its spectrum is almost indistinguishable from the spectra of two-phase intergrowths. On the other hand, there are two additional peaks in the spectrum of $Ks_{88}$, at ~920 and ~ 970 $cm^{-1}$, which are absent from the $Ks_{100}$ spectra. The intensity of the peak at ~380 $cm^{-1}$ is also different. Additional vibrational modes in this sample could be associated with its enlarged unit cell ($\sqrt{3}A \times \sqrt{3}A \times C$).

## DISCUSSION

### Structural variants

**The *nA* superstructures.** The multiple superstructures make an interesting set, with the repeat distance in the $a$-$b$ plane increasing with increasing $K^+$ content. Natural nepheline (~$Ne_{75}Ks_{25}$) has a basic $2A$ repeat and might

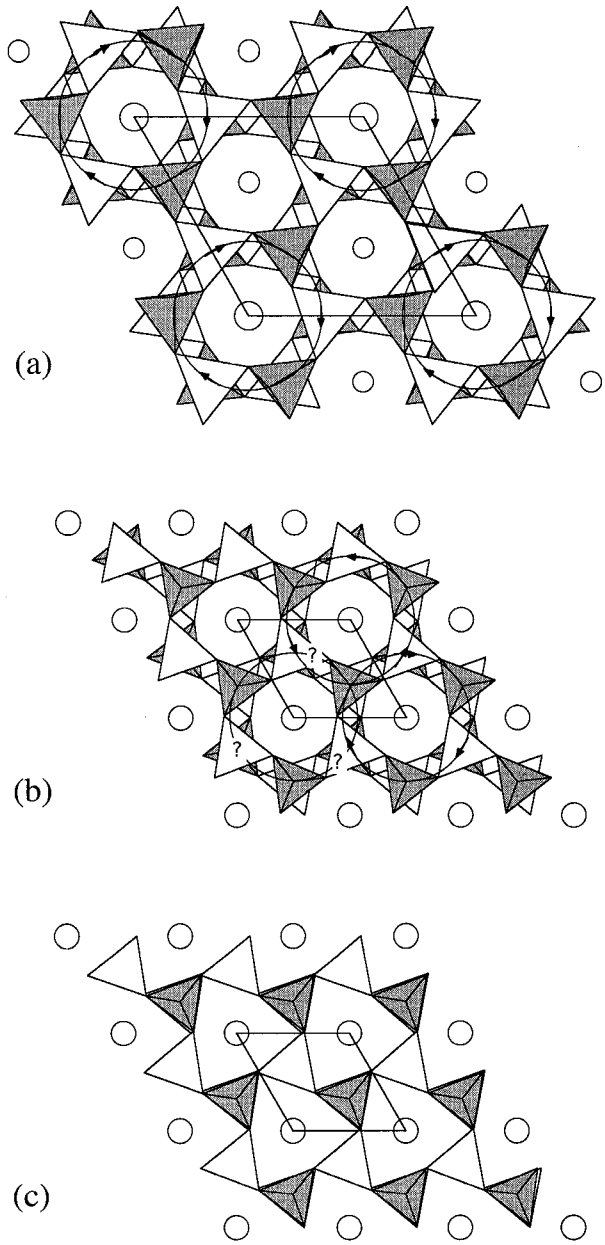


**FIGURE 16.** Kalsilite structures viewed down [001]; one unit cell is indicated in each case. **(a)** The $\sqrt{3}A$, $P6_3$ structure, after Barbier et al. (1993), showing that the ordering scheme for apical O atoms involves rotations about the $6_3$ axes located at the corners of the unit cell (atomic coordinates taken from Ga = Al substituted form). **(b)** The $1A$, $P6_3$ structure, after Andou and Kawahara (1984). If the same rotatory ordering scheme of the apical O atoms about one $6_3$ axis occurred, it would be compatible only with ordering in the opposite sense around the adjacent $6_3$ axis. The $6_3$ axis adjacent to both of these could not then have the same ordering as either. The system is frustrated, and, on average, has a disordered distribution of apical O atoms around the triad axis. **(c)** Hypothetical $P31c$ structure for kalsilite, derived by adopting atomic coordinates from the asymmetric unit of the $P6_3$ structure. Apical O atoms are probably disordered off the triad axes. Successive (001) layers have an eclipsed conformation, as opposed to the staggered conformation of the $1A$, $P6_3$ structure.

be thought of in this context as "dikalsilite." It has a distortion that permits complete ordering of $Na^+$ onto small sites and $K^+$ onto large sites, and, as discussed by Merlino (1984), the chemistry of trikalsilite and tetrakalsilite can be understood in analogous terms. The $6A$ superstructure represents the potassic end-member of this sequence, but it has a much more restricted occurrence. Indeed, it may develop only as an intergrowth sharing (001) with $1A$, $P6_3$ kalsilite because there is no possibility of stabilization by alkali ordering.

High tetrakalsilite, with $hhl$, $l$ = odd reflections absent (presumed to be $P6_3mc$), was identified for the first time in this study. It exists, apparently as an equilibrium state, above ~930 °C at $Ks_{88}$ and above ~870 °C at $\sim Ks_{74}$. Whether "hexakalsilite" has space group $P6_3$ or $P6_3mc$ is not yet certain, but, given that the multiple $A$ superstructures appear to develop during heating only when the $P6_3$ structure becomes unstable, $P6_3mc$ seems more likely. The line splitting reported by Capobianco and Carpenter (1989, their Fig. 5) as evidence that this phase is orthorhombic was at the limit of experimental resolution, and, given the new interpretation of a trigonal low-temperature phase, is now discounted.

**The $\sqrt{3}A$ structure.** In marked contrast with the multiple $A$ superstructures, extra reflections from the $\sqrt{3}A$ superstructure are diffuse, indicating relatively short-range correlations. The extra reflections are discs with a larger dimension in the $a^*$-$b^*$ plane than perpendicular to it. Within each crystal, APDs of the superstructure must be columnar in shape, with their long axes normal to the tridymite sheets (Fig. 12d). Smith and Sahama (1957) reported that annealing natural Nyiragongo specimens with this structure at 600 °C for 3 d caused the extra reflections to disappear. Alkalis are certainly mobile in nepheline and kalsilite at this temperature, and the change could be associated with varying composition as much as with a simple structural relaxation. In the present study, all crystals with compositions in the range $\sim Ks_{88-95}$ gave electron diffraction patterns containing these reflections, including $Ks_{88}$ crystals that had been annealed at 950 °C. Variations in the intensities of these reflections were found between crystals, but it seems likely that, although the most diffuse reflections might be overlooked in single-crystal X-ray diffraction patterns, all crystals of kalsilite containing 3–12 mol% Ne in solid solution have the $\sqrt{3}A$ structure at room temperature. The compositional range could be wider.

The $\sqrt{3}A$ superstructure is also found in crystals from the $(Na,K)GaSiO_4$ and $(Na,K)AlGeO_4$ solid solutions (Barbier and Fleet 1988; Barbier et al. 1993). Rietveld refinement of a member of the Ga solid solution by Barbier et al. (1993) confirmed that it is isostructural with $BaMSiO_4$ ($P6_3$), where M is Co, Zn, or Mg (Liu and Barbier 1993). Apart from the larger unit cell, the primary difference between the $\sqrt{3}A$, $P6_3$ structure (Fig. 16a) and the $1A$, $P6_3$ structure (Fig. 16b) is that in the former the apical O atoms linking successive tetrahedral sheets are displaced off the threefold rotation axes in a fully ordered array. A basic requirement for the stability of this struc-

ture in (Na,K) solid solutions containing combinations of Ga, Ge, and Si as the tetrahedral cations seems to be that there is some Na substitution for K away from the potassic end-member. The KGa and KGe phases do not even have a tridymite framework topology (Barbier and Fleet 1988; Barbier et al. 1993). The implication is, again, that a degree of Na-K ordering between two symmetrically distinct alkali sites may be required to stabilize the $\sqrt{3}A$ kalsilite form.

A parent tridymite structure for the $\sqrt{3}A$ structure may be MX-1, which has the same unit cell (Hoffmann et al. 1983; Carpenter and Wennemer 1985). Although some MX-1 tridymite is incommensurate (Hoffmann et al. 1983; Löns and Hoffmann 1987; Ashworth 1989), a commensurate form is also found (Withers et al. 1994), and the metric difference between the two is small. The same basic distortion may also occur at low temperatures in natural nepheline, though tripling of the unit cell along [110]* (of the $2A$ structure) is accompanied by an irrational repeat parallel to $c^*$ (Sahama 1958; McConnell 1962, 1981; Parker and McConnell 1971; Parker 1972; Merlino 1984). In nepheline the framework distortion is believed to be stabilized by K-vacancy ordering in the large cavity sites but is still restricted to a low-temperature stability field (Parker and McConnell 1971; Parker 1972; McConnell 1981, 1991). Other synthetic nepheline samples may have analogous distortions (Brown et al. 1972; Henderson and Roux 1977). A relationship with the dynamical properties of tridymite is also highlighted by the diffuse diffraction intensity from its high-temperature forms (e.g., Fig. 3a of Withers et al. 1994), which is very similar to the curved diffuse bands visible in Figure 11.

**The *P*31*c* structure.** This newly proposed structure occurs in end-member kalsilite from metamorphic rocks. Although a structure refinement has not yet been attempted, several strands of evidence support the suggestion that it is isostructural with the $P31c$ phase of $KLiSO_4$ described by Bansal et al. (1980), Zhang et al. (1988), Rajagopal et al. (1991), and Bhakay-Tamhane et al. (1985, 1991). Individual layers of this structure are essentially the same as those of the $1A$, $P6_3$ structure but are stacked in an eclipsed manner, as illustrated in Figure 16c. Apical O atoms still have their average positions on threefold symmetry axes.

Systematic absences and the pattern of dark-field images showing (001) twins observed by transmission electron microscopy are not consistent with the $Cmc2_1$ pseudohexagonal structure suggested by Capobianco and Carpenter (1989), but they are entirely consistent with an intergrowth of $P31c$ and $P6_3$ phases sharing (001) interfaces. Coexistence of these two structure types is characteristic of crystals of $KLiSO_4$ held below their $P6_3 \rightleftharpoons P31c$ transition temperature (Bhakay-Tamhane et al. 1985, 1991; Bhakay-Tamhane and Sequeira 1986; Perpétuo et al. 1992), whereas Sorge and Hempel (1986) and Klapper et al. (1987) have described the common occurrence of (001) twin boundaries in $P6_3$ crystals. Dollase and Freeborn (1977) also argued that (001) should be a low-energy interface between $P6_3$ twins in kalsilite. The same orientation of interface between trigonal and hexagonal structures might be favored because the apical O atoms would either match up perfectly or could accommodate slight misfits by tilting of the $SiO_4$ tetrahedra.

According to Mukhopadhyay et al. (1986, and see Bhakay-Tamhane et al. 1991), the intensities of reflections of the type *hhl* should be sensitive to the structural change $P6_3 \rightarrow P31c$. Those with $l$ = even would be expected to increase in intensity, whereas those with $l$ = odd should go to zero (and see calculated structure factors for kalsilite in Table 3). This explains the irreversible increase in $I_{111}$ and decrease in $I_{112}$ observed when the metamorphic kalsilite is converted to the $P6_3$ structure by annealing at temperatures greater than a few hundred degrees Celsius. Some intensity at the 111 peak positions in X-ray powder patterns from the starting material can be explained by the presence of $P6_3$ material intergrown with the $P31c$ phase. The two structures of $KLiSO_4$ have essentially the same IR spectra (Varma et al. 1990), which also accounts for the initially surprising observation that changing the proportion of $P6_3$ and $P31c$ kalsilite by annealing at 500 °C gives no change in the spectra of $Ks_{100}$ (Fig. 15).

Finally, the $P31c$ structure of $KLiSO_4$ has a slightly larger unit-cell volume and $c$ dimension than the $P6_3$ structure (Tomaszewski and Lukaszewicz 1983; Rajagopal et al. 1991). Annealing metamorphic $Ks_{100}$ above a few hundred degrees produces a small irreversible change in the same parameters, measured at room temperature (Fig. 3), with the hypothetical $P31c$ kalsilite also having slightly larger $V$ and $c$ parameters than $P6_3$ kalsilite. High-angle reflections in a Guinier X-ray powder diffraction pattern of the natural $Ks_{100}$ were examined for evidence of an intergrowth of phases with different $c$ parameters. The 006 ($2\theta \approx 64°$) and 108 ($2\theta \approx 93°$) reflections showed a slight asymmetry, consistent with a preponderance of material having $c \approx 8.72$ Å coexisting with a lesser component having $c \approx 8.71$ Å. The 220 reflection ($2\theta \approx 73°$) had a symmetrical intensity distribution. Heaney (personal communication, and see Moore and Reynolds 1989) pointed out that severe stacking disorder, such as occurs in turbostratically disordered clays, might also contribute to this asymmetry.

**Twinning.** Structure refinements of the hexagonal and trigonal phases of $KLiSO_4$ have had to consider the presence of merohedral twinning (Schulz et al. 1985; Zhang et al. 1988; Chen and Wu 1989; Bhakay-Tamhane et al. 1984, 1985, 1991). Pairs of twins in $P6_3$ structures are related by the former mirror plane parallel to the $c$ axis in $P6_3mc$, as are pairs of twins in the $P31c$ structure. If the twin boundaries and interphase boundaries are all parallel to (001), then some simple structural relationships result. For each structure, the sequence of tetrahedral layers follows the tridymite sequence ABABAB. Within a single layer the distortions from hexagonal to ditrigonal rings require that the triangles outlined by the tetrahedra all point in either one direction or in the opposite direction. These two senses of deformation can be

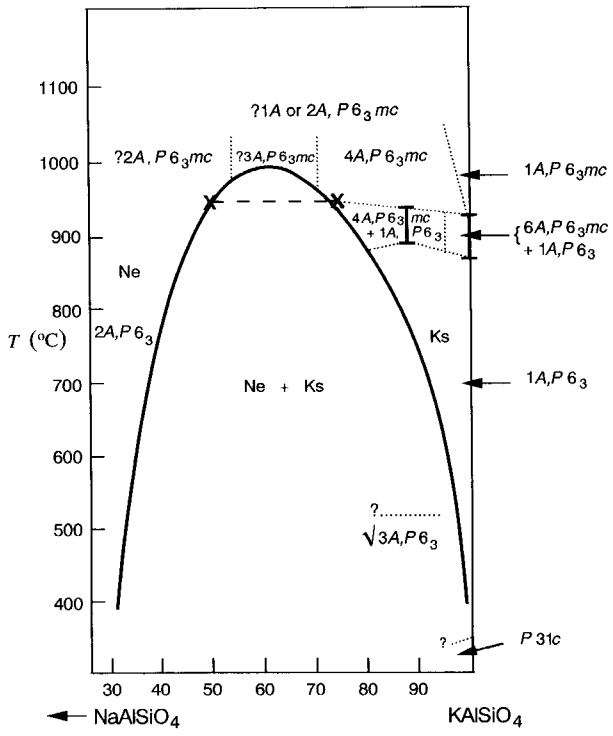


**FIGURE 17.** Schematic stability limits for different superstructures at the Ks-rich end of the Ne-Ks system. The solvus is from Figure 3 of Ferry and Blencoe (1978) (their version calculated on the basis of polybaric Margules equations); compositions of a Ne-Ks intergrowth annealed at 950 °C (Xs joined by a dashed line) are consistent with this solvus. I-shaped bars indicate the transition regimes of coexisting high- and low-temperature structures at $Ks_{88}$ and $Ks_{100}$. The dotted lines represent a self-consistent view of the effect of temperature and composition on the kalsilite structure; their positions are either poorly constrained or unconstrained, and no attempt was made to show them in a thermodynamically correct topology. At Ks-rich compositions, the stable high-temperature polymorph is O1 kalsilite (Tuttle and Smith 1958), but this is not shown.

described by adding a + or − superscript to the A and B labels, giving $A^+$, $A^-$, $B^+$, and $B^-$ as the possible layer conformations. One twin of the $P6_3$ structure is then characterized by the stacking sequence $A^+B^-A^+B^-A^+B^-$, whereas the second has $A^-B^+A^-B^+A^-B^+$. In the $P31c$ structure the ditrigonal prisms of every layer point in the same direction, giving sequences parallel to $c$ of $A^+B^+A^+B^+A^+B^+$ and $A^-B^-A^-B^-A^-B^-$ for the two twin components. A (001) twin boundary in $P6_3$ would thus be at the vertical line in $A^+B^-A^+B^- \mid A^-B^+A^-B^+$ (or, equivalently, reversing all the signs), and in the $P31c$ structure it would be at the vertical line in $A^+B^+A^+B^+ \mid A^-B^-A^-B^-$. On this schematic basis, the twin boundary in $P6_3$ is a unit of $P31c$ structure, and the twin boundary in $P31c$ is a unit of $P6_3$ structure. If the $P31c$ and $P6_3$ structures have only slightly different free energies, the boundaries would tend to be wider than only two layers and could be expected to persist as metastable defects for prolonged annealing times on either side of the $P6_3 \rightleftharpoons P31c$ equilibrium transition temperature.

One further observation is consistent with the suggestion that the excess energy associated with these defects might be small. Dollase and Freeborn (1977) deduced that kalsilite crystals produced by ion exchange of $K^+$ for $Na^+$ in nepheline contained abundant (001) twins. Formation of $1A$, $P6_3$ kalsilite in this way requires not only the compositional change but also a change from eclipsed to staggered layers. A coherent and persistent structure seems to result even if full reorganization of the stacking sequences is not achieved. It would not be surprising to find some $P31c$ layers in such crystals.

Merohedral twins are not generally expected to show strongly preferred boundary orientations because, by definition, they are not associated with any ferroelastic strain, as reviewed by Nord (1992). Structural arguments can be made to explain why (001) might be a particularly low-energy orientation in kalsilite and thus tend to cause alignment of the twin boundaries. Why {100} should also be a relatively low-energy orientation is not so obvious, though Dollase and Freeborn (1977) predicted that it might permit a minimal disturbance of the polyhedral connectivity. The merohedral twinning in nepheline exsolved from the Mount Nyiragongo kalsilite is much less regular. Most of the twin boundaries have no preferred orientation, but a low-energy interface is again evidently parallel to {100}. The (001) orientation is almost certainly unfavorable because the apical O atoms of $2A$, $P6_3$ twins would not match up across this plane.

## Stability relations

The new observations allow some updating of the stability relations for the Ks-rich side of the Ne-Ks system, following the work of Sahama (1957), Tuttle and Smith (1958), Ferry and Blencoe (1978), and Abbott (1984). The solvus shown in Figure 17 is the version calculated from the "polybaric Margules equations" by Ferry and Blencoe, which are constrained by a considerable amount of experimental data. Nepheline and kalsilite compositions in the sample of 75422 that equilibrated at 950 °C match this solvus closely. Stability limits for the different structure types are much less well defined and are shown only schematically in Figure 17. The ideal high-temperature structure with Al-Si disorder would have $P6_3/mmc$ symmetry (Abbott 1984; Kawahara et al. 1987) but is not included here because of the expectation that a high degree of Al-Si order is retained up to the melting points of all the phases in the system.

Most strikingly, the structural relationships do not conform to the simple symmetry hierarchy discussed by Abbott (1984). The known high-temperature phases (ignoring nontridymite structures, such as O1-$KAlSiO_4$) are $1A$, $P6_3mc$ high kalsilite and the multiple $A$ superstructures derived from this, which are shown speculatively to vary

with composition from nepheline ($2A$) to hexakalsilite ($6A$). Capobianco and Carpenter (1989) found coexisting $4A$ and $6A$ superstructure reflections in the single-crystal X-ray diffraction pattern of a crystal with composition $\sim Ks_{95}$ held at a high temperature, suggesting that the stability range for the $6A$ structure is restricted to compositions with Ks > 95 mol%. The nepheline structure could provide a more extensive high-$T$ solid solution (Sahama 1957), but the $1A$, $P6_3mc$ structure seems an equally likely candidate. Birefringence and thermal anomalies found by Sahama (1957) at ~1000 °C for a composition in the vicinity of $Ks_{75}$ perhaps indicate the lower temperature limit for this solid solution. In situ observations above 1000 °C are clearly needed.

At lower temperatures, $1A$, $P6_3$ kalsilite has the largest stability field according to the relations suggested in Figure 17. It gives way to $P31c$ kalsilite in the pure end-member phase at some temperature below ~200 °C if the upper stability limit implied by the single-crystal data in Figure 4 is accepted. Under equilibrium conditions, any $\sqrt{3}A$, $P6_3$ stability field would have to be rather narrow but could extend metastably into the solvus. Its upper temperature limit has not yet been investigated, though, as discussed below, the break in slope found in the $c$ parameter of $Ks_{88}$ at ~500 °C is a tempting point to place a $1A$, $P6_3 \rightleftharpoons \sqrt{3}A$, $P6_3$ transition.

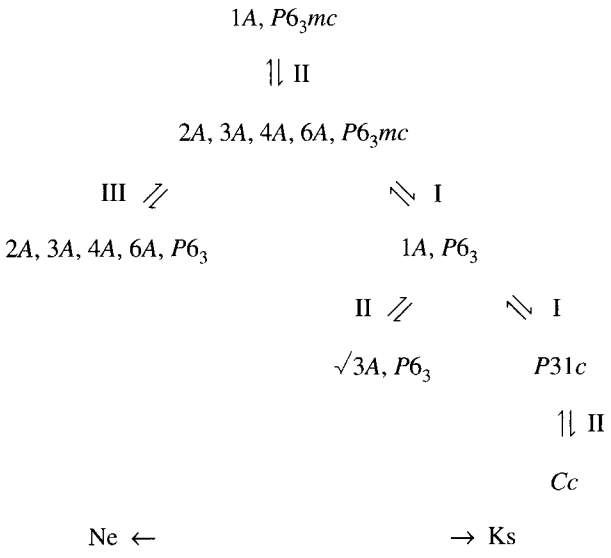


**FIGURE 18.** Schematic summary of isochemical transitions. Those on the right occur at more Ks-rich compositions, and those on the left at more Ne-rich compositions. Each transition is labeled: I = first-order character because the space groups do not have a supergroup → subgroup relationship; II = first-order character because third-order invariants of the order parameter are permitted in the excess free energy; III = thermodynamically continuous character permitted by symmetry.

## Phase transitions

A summary of isochemical phase transitions that might occur in kalsilite is shown in Figure 18. The lack of a consistent supergroup → subgroup hierarchy down the sequences requires that some of the transitions must be first order in character, even though the basic tridymite framework is common to all the phases. Transitions of the type $nA$, $P6_3mc \rightarrow 1A$, $P6_3$, where $n = 2, 3, 4, 6$, would involve a reduction in unit-cell size with falling temperature, for example, whereas the symmetry change $P6_3 \rightarrow P31c$ involves space groups that are subgroups of equal order with respect to the supergroup $P6_3mc$. They are designated as type I in Figure 18 and must occur by means of nucleation and growth mechanisms. They appear to be characterized by substantial hysteresis effects, with large temperature intervals of two coexisting phases. Single crystals of kalsilite develop two-phase intergrowths at the high-temperature transitions (this study), while the same behavior is displayed at the $P6_3 \rightleftharpoons P31c$ transition in single crystals of $KLiSO_4$ (Bhakay-Tamhane et al. 1991; Perpétuo et al. 1992). Henderson and Taylor (1982) explained the coexistence of two isochemical phases over a significant temperature interval in the analogous systems $BaAl_2O_4$ and $Sr_2AlO_4$ by making a comparison with martensitic transitions. The apparent violation of the phase rule can be accounted for if strain acts as an additional degree of freedom.

A second set of transitions has supergroup → subgroup relationships, but each transition is required to be first order in character because of the existence of third-order invariants of the order parameter in their excess free energies. From the symmetry properties listed in the tables of Stokes and Hatch (1988) these include the $1A$, $P6_3mc \rightleftharpoons nA$, $P6_3mc$ and $1A$, $P6_3 \rightleftharpoons \sqrt{3}A$, $P6_3$ transitions labeled type II in Fig. 18. Only the $nA$, $P6_3mc \rightleftharpoons nA$, $P6_3$ transitions, where n has the same value above and below the transition point, are not excluded by symmetry from being thermodynamically continuous (type III in Fig. 18). An example of the latter has not yet been observed but must occur in tetrakalsilite somewhere between ~950 °C, where it probably has $P6_3mc$ symmetry (this study), and room temperature, where it has $P6_3$ symmetry (Merlino et al. 1985). If the $1A$, $P6_3mc \rightleftharpoons 1A$, $P6_3$ transition in pure kalsilite, the "high" ⇌ "low" transition of Andou and Kawahara (1982) and Kawahara et al. (1987), occurred without the appearance of the intermediate $6A$ structure, it too could be thermodynamically continuous according to symmetry arguments alone.

With regard to the thermodynamic driving forces behind all these transitions, four processes have been considered: Al-Si ordering, Na-K ordering, displacements of basal O atoms, and displacements of the apical O atoms. All the available evidence (reviewed by Palmer 1994) is consistent with a high degree of Al-Si order being maintained up to the solidus of the Ne-Ks system. Other framework structures with 1:1 ratios of Al:Si tend to have high transition temperatures; in anorthite the extrapolated transition temperature is ~2000 °C, for example (Car-

penter and McConnell 1984). Large ordering energies equate with high transition temperatures, and Al-Si disordering can probably be ruled out as having any significant influence on the thermal evolution of natural kalsilite.

The second possible driving mechanism is Na-K ordering. The trend of increasing values of $n$ with increasing Ks content in the $nA$, $P6_3mc$ superstructures discussed earlier is presumably dictated by the need of the framework to accommodate cations that differ in ionic radius by ~30%. Transitions from $1A$, $P6_3mc$ to $nA$, $P6_3mc$ structures could therefore be driven by Na-K ordering, but their transition temperatures are as yet unknown and might fall above the liquidus.

Transitions from $P6_3mc$ structures to $P6_3$ structures are driven primarily by ordering of basal O atoms between two sites in each (001) layer, which are displaced off the mirror planes parallel to c of the ideal $1A$, $P6_3mc$ structure (Dollase and Freeborn 1977; Andou and Kawahara 1982; Kawahara et al. 1987). Different patterns of such displacements can largely account for the differences between low kalsilite, low trikalsilite, and low tetrakalsilite, for example. The fact that the $1A$, $P6_3$ structure, which has only one distinct alkali site, becomes stable with respect to $nA$ structures below ~900 °C, between ~$Ks_{100}$ and ~$Ks_{70}$, implies that the energy of the local O-atom ordering scheme in this structure outweighs the energy of Na-K ordering. Alkali ordering also cannot be responsible for driving the $P6_3 \rightleftharpoons P31c$ transition in pure $KAlSiO_4$. These staggered and eclipsed forms differ overtly only in their basal O-atom ordering schemes, and some small energetic difference between the two ordered configurations could account for the transition. A valid analogy is almost certainly that of polytypic systems because they have such a strongly preferred interfacial orientation.

Ordering of the apical O atoms appears to occur at the low-temperature limits of the sequences in Figure 18. In a discussion of $KLiSO_4$, Pimenta et al. (1989) pointed out that the O atoms that form the bases of tetrahedra in stuffed tridymite phases lie within a densely packed plane, whereas those at the apices linking successive sheets are much less restricted. Librational motions of the tetrahedra about axes parallel to $c$, which would give displacements of the basal O atoms between the ordering positions, should therefore be subject to larger restoring forces than motions about axes perpendicular to $c$, which would cause the apical O-atom displacements. Accordingly, the energies of the latter are expected to be relatively low, consistent with the low ordering temperatures. The $1A$, $P6_3$ structure has apical O-atom disorder (Perrotta and Smith 1965; Dollase and Freeborn 1977; Andou and Kawahara 1984; $KLiSO_4$: Karppinen et al. 1983; Bhakay-Tamhane et al. 1984, 1991; Schulz et al. 1985), but the $\sqrt{3}A$, $P6_3$ structure has complete order (Fig. 16a) (Barbier et al. 1993; Liu and Barbier 1993). The preferred ordering scheme involves the tilting of tetrahedra in a rotatory fashion around the $6_3$ axes (Fig. 16a). An equivalent scheme in the $1A$, $P6_3$ structure is impossible because of a frustration effect: Rotatory ordering about one $6_3$ axis requires rotatory ordering in exactly the opposite sense about the adjacent $6_3$ axis. The $6_3$ axis adjacent to both of the first two cannot then adopt the same scheme in either sense (Fig. 16b). Some additional process is required to break the translational symmetry, and a small proportion of Na substitution for K appears to allow this to occur. Triggering of the $1A$, $P6_3 \rightleftharpoons \sqrt{3}A$, $P6_3$ transition thus seems to involve coupling of the apical O-atom displacements with some Na-K ordering.

In $KLiSO_4$, the apical O-atom ordering causes a symmetry reduction from $P6_3$ to a monoclinic (pseudoorthorhombic) $Cc$ structure (Bhakay-Tamhane and Sequeira 1986; Dantas et al. 1991; Rajagopal et al. 1991; Bhakay-Tamhane et al. 1991; Perpétuo et al. 1992). The ordering scheme has all apical O atoms within the same (001) plane displaced in a single direction rather than in a rotatory manner (Bhakay-Tamhane et al. 1991). The existence of an equivalent $P31c \rightleftharpoons Cc$ transition might reasonably be predicted for pure kalsilite below room temperature. It must be first order because of the existence of third-order invariants, and it would be expected to show hysteresis and two-phase coexistences just as has been observed in $KLiSO_4$ by Bhakay-Tamhane and Sequeira (1986), Bhakay-Tamhane et al. (1991), Rajagopal et al. (1991), and Perpétuo et al. (1992). An analogous transition in structures with staggered rather than eclipsed sequences of layers is the $P6_3 \rightleftharpoons P2_1$ transition observed in $SrAl_2O_4$, which displays similar first-order behavior (Henderson and Taylor 1982). In the $P2_1$ structure, the apical O atoms in a single (001) plane are displaced in a zigzag manner about the $b$ axis (Schulze and Müller-Buschbaum 1981).

The rigid-unit modes of ideal high-temperature tridymite were recently calculated by Dove et al. (1996). They found lines of rigid-unit modes along $a^*$ and along $[110]^*$, including the special points 0,0,0, ⅓,⅓,0, and ½,0,0, and curved surfaces elsewhere in reciprocal space. Some of the kalsilite transitions could therefore conform to a rigid-unit-mode type of displacive mechanism. The close relationships with MX-1 tridymite, Ge and Ga derivatives of Ne and Ks, and among patterns of diffuse scattering in tridymite, nepheline, and kalsilite certainly point to a strong control by the underlying framework. However, purely displacive mechanisms ought to give more regular supergroup-subgroup symmetry hierarchies. Jumping from one structure type to another in a seemingly erratic manner is more characteristic of thermodynamic control by order-disorder phenomena. Competition between ordering processes could result in diverse structures stable only over restricted temperature and compositional intervals if the most favorable configuration for each of the separate Na-K, basal O-atom, and apical O-atom distributions is not entirely compatible with the most favorable configurations of the others. In other words, there are several possible couplings between individual displacive and order-disorder processes that lead

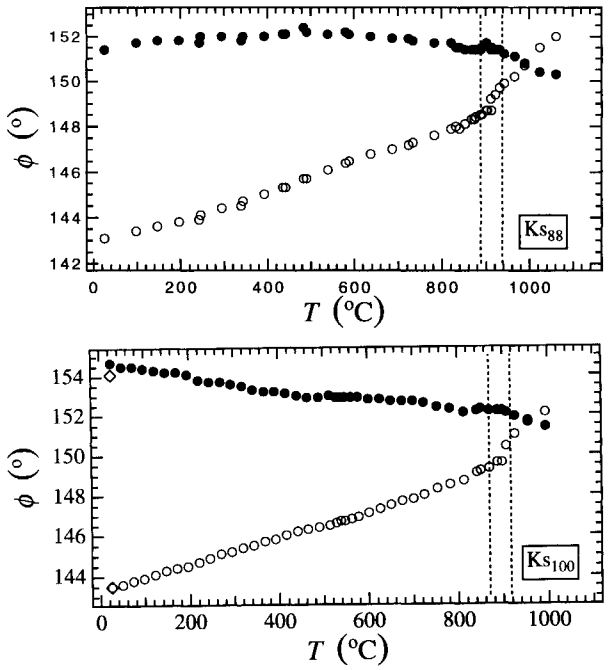


FIGURE 19. Temperature evolution of $\phi_a$, the intrasheet Si-O-Al angle (open circles), and $\phi_c$, the intersheet Si-O-Al angle (solid circles), for $Ks_{100}$ and homogenized $Ks_{88}$. These angles were calculated from the $a$ and $c$ lattice-parameter data using the geometrical relations given in the text (after Capobianco and Carpenter 1989). Vertical dashed lines indicate the temperature limits of two-phase fields. Open diamonds indicate values of $\phi_a$ and $\phi_c$ for $Ks_{100}$ after cooling from high temperatures.

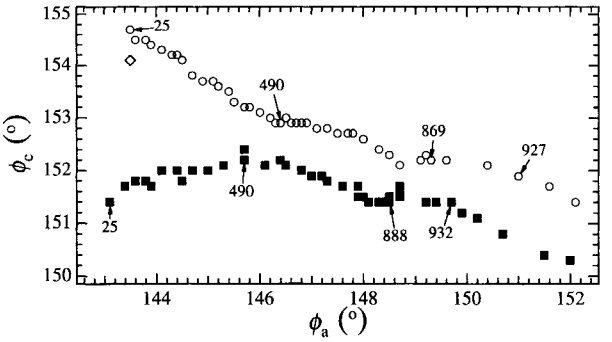


FIGURE 20. Variation of $\phi_c$ as a function of $\phi_a$. From ~1060 °C (bottom right) to ~500 °C, the $Ks_{88}$ and $Ks_{100}$ data follow parallel trends. Below ~500 °C the trends diverge, perhaps as a consequence of the phase transition $1A$, $P6_3 \rightleftharpoons \sqrt{3}A$, $P6_3$ in the $Ks_{88}$ sample. Open diamond = $Ks_{100}$ after cooling from high $T$.

to different structures with only marginally different energies.

### Al-O-Si bond angles

The source of driving energies for O-atom positional ordering can be understood in terms of Al-O-Si bond angles in stuffed tridymite framework topologies. In ideal, fully expanded tridymite, all T-O-T bond angles are 180°, where T is the tetrahedral cation. Within (001) sheets every pair of tetrahedra is in the trans configuration, and all pairs linking sheets are in the cis configuration (as reviewed most recently by Heaney 1994, for example). Numerous studies have demonstrated that framework structures with any degree of flexibility are unlikely ever to match this limiting case (e.g., Gibbs et al. 1981; Geisinger et al. 1985; Navrotsky et al. 1985; Liebau 1985; Lasaga and Gibbs 1987). Apparent 180° angles can only be due to averaging over different O-atom positions, but determination of the true atomic distributions is not straightforward. Some insights into how the average T-O-T angles vary with temperature are, however, provided by variations in the lattice parameters. Capobianco and Carpenter (1989) derived approximate geometrical dependencies for the Al-O-Si angle of tetrahedra linked within a sheet on the $a$ lattice parameter, $\phi_a$, and for the angle of tetrahedra forming the linkage between sheets on $c$, $\phi_c$, with the mean Si-O and Al-O bond lengths specified as $d_{Si}$ and $d_{Al}$. For $1A$ structures these are

$$\cos \phi_a = -\left[\frac{\frac{a^2}{3} + \left(\frac{1}{9}\right)(d_{Al} + d_{Si})^2 - d_{Al}^2 - d_{Si}^2}{2d_{Al}d_{Si}}\right]$$

$$\cos \phi_c = -\left[\frac{\frac{c^2}{4} - \left(\frac{16}{9}\right)(d_{Al}^2 + d_{Si}^2)}{\left(\frac{32}{9}\right)d_{Al}d_{Si}}\right].$$

[Note that the equation for $\phi_c$ given by Capobianco and Carpenter (1989) contains two typographical errors.] Values of $\phi_a$ and $\phi_c$ were calculated using the lattice-parameter data in Table 1 and values of $d_{Al} = 1.74$, $d_{Si} = 1.61$ Å from Perrotta and Smith (1965). The latter are also close to the average values for trikalsilite (Bonaccorsi et al. 1988) and tetrakalsilite (Merlino et al. 1985), but the precise choice of tetrahedral bond lengths does not influence the overall pattern of results displayed in Figures 19 and 20. At room temperature the $a$ and $c$ parameters of $P6_3$ $Ks_{100}$ give $\phi_a = 143.5°$, $\phi_c = 154.1°$ and an average Al-O-Si bond angle for the complete structure of $\frac{1}{4}(\phi_c + 3\phi_a) = 146.2°$. This compares with 147°, estimated on the basis of the chemical shift for $^{27}Al$ NMR spectra from crystals containing ~94% Ks and its correlation with Al-O-Si angle given by Hovis et al. (1992; their Figs. 6 and 8). The structure refinement of a natural kalsilite (also not with pure end-member composition) by Perrotta and Smith (1965) gave $\phi_a = 140$, $\phi_c = 163°$ and an average of 146° (from Liebau 1985).

The results in Figure 19 show that the high-temperature $P6_3mc$ structures have $\phi_a > \phi_c$ (though the equations are strictly valid only for the $1A$ structure). A geometrical degeneracy, $\phi_a = \phi_c$, appears to coincide with the stability

limit with respect to the $1A$, $P6_3$ phase. A second, much smaller anomaly occurs in the bond-angle data at ~500 °C for both $Ks_{88}$ and $Ks_{100}$. In $Ks_{100}$ it coincides with a change in the slope of $V$ as a function of temperature (Fig. 3c) and, perhaps, in the width of the 111 reflection (Fig. 6). A break in slope of the lattice parameters at ~600 °C was also found by Kawahara et al. (1987) for a synthetic kalsilite, whereas the data of Henderson and Taylor (1988) show a change in slope of $V$ at ~450 °C for a different synthetic sample. There is no evidence for a change in macroscopic symmetry at this point, however, and some local short-range effects, which remain to be identified, may be implicated. The anomaly at ~500 °C for $Ks_{88}$ is more distinct (Fig. 19) and is even more evident if $\phi_c$ is plotted against $\phi_a$ (Fig. 20). With falling temperature the intersheet hinge angle, $\phi_c$, increases antipathetically with the intrasheet angle, $\phi_a$, in an almost identical manner for both $Ks_{88}$ and $Ks_{100}$ down to ~500 °C. The data for $Ks_{88}$ then diverge markedly from this trend, and it is tempting to invoke the onset of the $1A$, $P6_3 \rightleftharpoons \sqrt{3}A$, $P6_3$ transition. An additional degree of freedom due to the loss of translational symmetry perhaps permits not only the apical O-atom ordering but also a more coherent deformation mechanism for the framework, with both $\phi_a$ and $\phi_c$ decreasing with falling temperature.

### Microstructural evolution

End-member kalsilite has only been found in metamorphic rocks. A crystallization temperature of ~700–800 °C for the Indian sample (Sandiford and Santosh 1991) would be below the $6A$, $P6_3mc$ (or $P6_3$?) $\rightleftharpoons$ $1A$, $P6_3$ transition temperature. Twins related by the mirror plane parallel to the $c$ axis in $P6_3mc$ would be incorporated only as growth defects, therefore, but if they did occur they would presumably adopt twin boundaries parallel to (001). During slow cooling, the transition $P6_3 \rightarrow P31c$ would have been initiated at some temperature below ~200 °C by a nucleation and growth mechanism. Any (001) twin boundaries already present should provide prime nucleation sites given their local resemblance to the $P31c$ structure. Growth fronts from these or from nuclei at grain boundaries might be expected to advance most easily in directions perpendicular to the $c$ axis, giving a polytype-like, layer-by-layer change from $P6_3$ to $P31c$. The sluggishness of this process appears to be such that, even on a metamorphic time scale, the transition did not go to completion, and the proposed $P6_3 + P31c$ intergrowth was preserved as a kinetically stranded state. The absence of an equivalent microstructure in $Ks_{97}$ from sample 90049 is due either to the stability of the alternative $\sqrt{3}A$, $P6_3$ structure when a small amount of Na is present or to the relatively fast rate of cooling of this volcanic sample.

For crystals with compositions of ~$Ks_{88}$, such as in the Alban Hills sample, crystallization between ~930 °C and at least 1060 °C would cause the initial growth of high tetrakalsilite. The $4A$, $P6_3mc$ structure would then transform by nucleation and growth to $1A$, $P6_3$ kalsilite on cooling below ~890–930 °C. $P6_3$ twins would be expected to develop at this stage, but there is no evidence that their boundaries could be stabilized by effects associated with a potential $P31c$ phase, as in $Ks_{100}$. The twins might coarsen rapidly, therefore, and twin boundaries are certainly rare in the final product. The onset of nepheline exsolution would be expected at ~750–800 °C (Fig. 17); the scale of exsolution in natural samples is too coarse to yield evidence of the initial mechanism [spinodal decomposition, homogeneous nucleation, etc., as discussed by Yund et al. (1972)]. Stress fields set up by the ~5% volume difference between nepheline as a component in solid solution and as a separate phase probably generated many dislocations. Whether recovery of these dislocations, or stresses associated with some change in the preferred orientation of Ne-Ks interfaces as a function of temperature, could yield the polygonized texture remains to be determined. At some early stage in the exsolution process, the nepheline lamellae would also have had to undergo a transition from $1A$, $P6_3$ to $2A$, $P6_3$. The occasional linear defects imaged in dark field may be antiphase boundaries that developed at this stage, but they could also be stacking faults resulting from the passage of partial dislocations. Finally, the Ks-rich phase would have transformed from $1A$, $P6_3$ to $\sqrt{3}A$, $P6_3$, perhaps near ~500 °C. The dimensions of individual domains of the new superstructure remained restricted.

Exsolution in bulk compositions nearer to ~$Ks_{70}$ leaves a rather different microstructure. The onset of exsolution would have been at ~975 °C, within or above the two-phase field of $1A$, $P6_3 + 4A$, $P6_3mc$ phases (Fig. 17). There would still have been a significant volume change to accommodate, but the stresses could have been dispersed more evenly at the higher temperatures, such that the nepheline lamellae did not become polygonized. Stability relations for $2A$, $3A$, and $4A$ superstructures at the top of the solvus have not yet been investigated, but it is possible that the first nepheline to equilibrate at high temperatures also had a $P6_3mc$ structure. On cooling the Ne limb of the solvus, this would have transformed, perhaps by means of a $2A$, $P6_3mc \rightarrow 2A$, $P6_3$ transition, to the normal nepheline structure. This transition would be expected to generate merohedral twins in much the same manner as discussed by Abbott (1984) for a hypothetical $1A$, $P6_3mc \rightarrow 1A$, $P6_3$ transition in kalsilite. The twinning observed in nepheline from sample numbers 75422 and 90049 is at least consistent with this interpretation, especially as similar twinning was observed in tetrakalsilite, which must have undergone a $4A$, $P6_3mc \rightarrow 4A$, $P6_3$ transition during cooling from 950 °C.

In pyroxenes and feldspars a diversity of microstructures is related to the constraints of kinetics and cooling rates. In nepheline and kalsilite, Na $\rightleftharpoons$ K diffusion is sufficiently rapid that optical-scale exsolution occurs even in volcanic samples, but variable microstructures can still be generated because so many different transition sequences are possible. In principle the microstructures should also provide information relating to the thermal

history of the host rock. Observations on samples from a greater diversity of compositions and geological environments should be revealing, both of the effects of thermal history and of other possible structural sequences or transition mechanisms.

## Acknowledgments

D.C. acknowledges the receipt of a Fellowship from the Human Capital and Mobility program of the European Union and support from the Ministero dell' Universita e della Ricerca Scientifica e Tecnologica, Italy. M.A.C. acknowledges the receipt of a Leverhulme Trust Senior Research Fellowship from The Royal Society. We also thank A. Cundari, M. Sandiford, and M. Santosh for generously providing samples, C. Capobianco for continued help with the Ne-Ks system, D.C. Palmer for generating crystal-structure drawings (using equipment funded by NERC, grant no. GR9/1285, and The Royal Society, grant no. 14906), Ming Zhang for help with IR spectroscopy, and P. Burns for performing the structure-factor calculations. C.M.B. Henderson and P. Heaney kindly undertook the unenviable task of reviewing the manuscript, and their (much appreciated) critical comments led to several improvements and clarifications.

## References cited

Abbott, R.N., Jr. (1984) $KAlSiO_4$ stuffed derivatives of tridymite: Phase relationships. American Mineralogist, 69, 449–457.

Andou, Y., and Kawahara, A. (1982) The existence of high-low inversion point of kalsilite. Mineralogical Journal, 11, 72–77.

——— (1984) The refinement of the structure of synthetic kalsilite. Mineralogical Journal, 12, 153–161.

Ashworth, J.R. (1989) Transmission electron microscopy of coexisting low-tridymite polymorphs. Mineralogical Magazine, 53, 89–97.

Aurisicchio, C., and Federico, M. (1985) Nepheline-kalsilite microperthites in ejecta from the Alban Hills (Italy). Bulletin of the Geological Society of Finland, 57, 129–137.

Bannister, F.A., and Hey, M.H. (1931) A chemical, optical, and X-ray study of nepheline and kaliophilite. Mineralogical Magazine, 22, 569–608.

Bansal, M.L, Deb, S.K., Roy, A.P., and Sahni, V.C. (1980) New phase transition in $LiKSO_4$. Solid State Communications, 36, 1047–1050.

Barbier, J., and Fleet, M.E. (1988) Investigation of phase relations in the $(Na,K)AlGeO_4$ system. Physics and Chemistry of Minerals, 16, 276–285.

Barbier, J., Liu, B., and Weber, J. (1993) Crystal chemistry of the $(Na,K)GaSiO_4$ system. European Journal of Mineralogy, 5, 297–305.

Barbieri, M., Federico, M., and Tolomeo, L. (1970) Contributi alla conoscenza della caliofilite in relazione a recenti ritrovamenti. Periodico di Mineralogia, 39, 323–341.

Bhakay-Tamhane, S., Sequeira, A., and Chidambaram, R. (1984) Structure of lithium potassium sulphate, $LiKSO_4$: A neutron diffraction study. Acta Crystallographica, C40, 1648–1651.

——— (1985) Low-temperature phase transitions in $LiKSO_4$: A neutron study. Solid State Communications, 53, 197–200.

Bhakay-Tamhane, S., and Sequeira, A. (1986) Kinetics and symmetry changes in low-temperature phase transitions in $LiKSO_4$. Ferroelectrics, 69, 241–251.

Bhakay-Tamhane, S., Sequeira, A., and Chidambaram, R. (1991) Phase transitions in $LiKSO_4$: Low-temperature neutron diffraction results. Phase Transitions, 35, 75–98.

Bonaccorsi, E., Merlino, S., and Pasero, M. (1988) Trikalsilite: Its structural relationships with nepheline and tetrakalsilite. Neues Jahrbuch für Mineralogie Monatshefte, 559–567.

Brown, W.L., Cesbron, F., and Dupont, G. (1972) Trinepheline: A new synthetic modification in the nepheline group. Zeitschrift für Kristallographie, 136, 468–470.

Buerger, M.J., Klein, G.E., and Donnay, G. (1954) Determination of the crystal structure of nepheline. American Mineralogist, 39, 805–818.

Capobianco, C., and Carpenter, M. (1989) Thermally induced changes in kalsilite ($KAlSiO_4$). American Mineralogist, 74, 797–811.

Carpenter, M.A., and McConnell, J.D.C. (1984) Experimental delineation of the $C\bar{1} \rightleftharpoons I\bar{1}$ transformation in intermediate plagioclase feldspars. American Mineralogist, 69, 112–121.

Carpenter, M.A., and Wennemer, M. (1985) Characterization of synthetic tridymites by transmission electron microscopy. American Mineralogist, 70, 517–528.

Cellai, D., Carpenter, M.A., and Heaney, P.J. (1992) Phase transitions and microstructures in natural kaliophilite. European Journal of Mineralogy, 4, 1209–1220.

Cellai, D., Carpenter, M.A., Wruck, B., and Salje, E.K.H. (1994) Characterization of high-temperature phase transitions in single crystals of Steinbach tridymite. American Mineralogist, 79, 606–614.

Chen, R.H., and Wu, R.T. (1989) An X-ray diffraction study of structural phase transitions of lithium potassium sulphate. Journal of Physics: Condensed Matter, 1, 6913–6920.

Dantas, M.S.S., Perpetuo, G.J., Nogueira, R.A., and Pimenta, M.A. (1991) Symmetry analysis of the ferroelastic phase in $LiKSO_4$. Ferroelectrics, 124, 397–402.

Dollase, W.A. (1970) Least-squares refinement of the structure of a plutonic nepheline. Zeitschrift für Kristallographie, 132, 27–44.

Dollase, W.A., and Peacor, D.R. (1971) Si-Al ordering in nephelines. Contributions to Mineralogy and Petrology, 30, 129–134.

Dollase, W.A., and Freeborn, W.P. (1977) The structure of $KAlSiO_4$ with $P6_3mc$ symmetry. American Mineralogist, 62, 336–340.

Dove, M.T., Hammonds, K.D., Heine, V., Withers, R.L., Xiao, Y., and Kirkpatrick, R.J. (1996) Rigid unit modes in the high-temperature phase of $SiO_2$ tridymite: Calculations and electron diffraction. Physics and Chemistry of Minerals, 23, 56–62.

Federico, M. (1976) On a kalsilitolite from the Alban Hills, Italy. Periodico di Mineralogia, 45, 5–12.

Ferry, J.M., and Blencoe, J.G. (1978) Subsolidus phase relations in the nepheline-kalsilite system at 0.5, 2.0, and 5.0 kbar. American Mineralogist, 63, 1225–1240.

Foreman, N., and Peacor, D.R. (1970) Refinement of the nepheline structure at several temperatures. Zeitschrift für Kristallographie, 132, 45–70.

Geisinger, K.L., Gibbs, G.V., and Navrotsky, A. (1985) A molecular orbital study of bond length and angle variations in framework structures. Physics and Chemistry of Minerals, 11, 266–283.

Gibbs, G.V., Meagher, E.P., Newton, M.D., and Swanson, D.K. (1981) A comparison of experimental and theoretical bond length and angle variations for minerals, inorganic solids and molecules. In M. O'Keefe and A. Navrotsky, Eds., Structure and bonding in crystals (1st edition), p. 195–225. Academic, New York.

Gregorkiewitz, M., and Schäfer, H. (1980) The structure of $KAlSiO_4$-kaliophilite-O1: Application of the subgroup-supergroup relations to the quantitative space group determination of pseudosymmetric crystals. Sixth European Crystallographic meeting, Barcelona, July 28–August 1, Abstracts, p. 155.

Hahn, Th., and Buerger, M.J. (1955) The detailed structure of nepheline, $KNa_3Al_4Si_4O_{16}$. Zeitschrift für Kristallographie, 106, 308–338.

Heaney, P.J. (1994) Structure and chemistry of the low-pressure silica polymorphs. In Mineralogical Society of America Reviews in Mineralogy, 29, 1–40.

Henderson, C.M.B., and Roux, J. (1977) Inversions in sub-potassic nephelines. Contributions to Mineralogy and Petrology, 61, 279–298.

Henderson, C.M.B., and Taylor, D. (1982) The structural behaviour of the nepheline family: (1) Sr and Ba aluminates ($MAl_2O_4$). Mineralogical Magazine, 45, 111–127.

——— (1988) The structural behaviour of the nepheline family: (3) Thermal expansion of kalsilite. Mineralogical Magazine, 52, 708–711.

Hoffmann, W., Kockmeyer, M., Löns, J., and Vach, C. (1983) The transformation of monoclinic low-tridymite MC to a phase with an incommensurate superstructure. Fortschritte der Mineralogie, 61, 96–98.

Hovis, G.L., Spearing, D.R., Stebbins, J.F., Roux, J., and Clare, A. (1992) X-ray powder diffraction and $^{23}Na$, $^{27}Al$, and $^{29}Si$ MAS-NMR investigation of nepheline-kalsilite crystalline solutions. American Mineralogist, 77, 19–29.

Karppinen, M., Lundgren, J.-O., and Liminga, R. (1983) Structure of pyroelectric lithium potassium sulphate, $LiKSO_4$. Acta Crystallographica, C39, 34–38.

Kawahara, A., Andou, Y., Marumo, F., and Okuno, M. (1987) The crystal

structure of high temperature form of kalsilite ($KAlSiO_4$) at 950 °C. Mineralogical Journal, 13, 260–270.

Klapper, H., Hahn, Th., and Chung, S.J. (1987) Optical, pyroelectric and X-ray topographic studies of twin domains and twin boundaries in $KLiSO_4$. Acta Crystallographica, B43, 147–159.

Lange, R.A., Carmichael, I.S.E., and Stebbins, J.F. (1986) Phase transitions in leucite ($KAlSi_2O_6$), orthorhombic $KAlSiO_4$, and their iron analogues ($KFeSi_2O_6$, $KFeSiO_4$). American Mineralogist, 71, 937–945.

Lasaga, A.C., and Gibbs, G.V. (1987) Applications of quantum mechanical potential surfaces to mineral physics calculations. Physics and Chemistry of Minerals, 14, 107–117.

Liebau, F. (1985). Structural chemistry of silicates, 347 p. Springer-Verlag, Berlin.

Lippmaa, E., Mägi, M., Samoson, A., Engelhardt, G., and Grimmer, A.-R. (1980) Structural studies of silicates by solid-state high-resolution $^{29}Si$ NMR. Journal of the American Chemical Society, 102, 4889–4893.

Liu, B., and Barbier, J. (1993) Structures of the stuffed tridymite derivatives, $BaMSiO_4$ (M = Co, Zn, Mg). Journal of Solid State Chemistry, 102, 115–125.

Löns, J., and Hoffmann, W. (1987) Zur Kristallstruktur der inkommensurablen Raumtemperaturphase des Tridymits. Zeitschrift für Kristallographie, 178, 141–143.

Lukesh, J.S., and Buerger, M.J. (1942) The unit cell and space group of kaliophilite. American Mineralogist, 27, 226–227.

McConnell, J.D.C. (1962) Electron-diffraction study of subsidiary maxima of scattered intensity in nepheline. Mineralogical Magazine, 33, 114–124.

——— (1981) Time-temperature study of the intensity of satellite reflections in nepheline. American Mineralogist, 66, 990–996.

——— (1991) Incommensurate structures. Philosophical Transactions of the Royal Society of London, A334, 425–437.

Merlino, S. (1984) Feldspathoids: Their average and real structures. In W.L. Brown, Ed., Feldspars and feldspathoids. NATO ASI series C, vol. 137, p. 435–470. Reidel, Dordrecht, the Netherlands.

Merlino, S., Franco, E., Mattia, C.A., Pasero, M., and De Gennaro, M. (1985) The crystal structure of panunzite (natural tetrakalsilite). Neues Jahrbuch für Mineralogie Monatshefte, 322–328.

Moore, D.M., and Reynolds, R.C., Jr. (1989) X-ray diffraction and the identification and analysis of clay minerals, 332 p. Oxford University Press, Oxford.

Mukhopadhyay, R., Paranjpe, S.K., and Bhakay-Tamhane, S. (1986) Powder neutron diffraction study of low temperature phase transition in $LiKSO_4$. Solid State Communications, 58, 203–204.

Navrotsky, A., Geisinger, K.L, McMillan, P., and Gibbs, G.V. (1985) The tetrahedral framework in glasses and melts: Inferences from molecular orbital calculations and implications for structure, thermodynamics and physical properties. Physics and Chemistry of Minerals, 11, 284–298.

Nord, G.L., Jr. (1992) Imaging transformation-induced microstructures. In Mineralogical Society of America Reviews in Mineralogy, 27, 455–508.

Palmer, D.C. (1994) Stuffed derivatives of the silica polymorphs. In Mineralogical Society of America Reviews in Mineralogy, 29, 83–122.

Parker, J.M. (1972) The domain structure of nepheline. Zeitschrift für Kristallographie, 136, 255–272.

Parker, J.M., and McConnell, J.D.C. (1971) Transformation behaviour in the mineral nepheline. Nature Physical Science, 234, 178–179.

Perpétuo, G.J., Dantas, M.S.S., Gazzinelli, R., and Pimenta, M.A. (1992) Low-temperature sequence of phase transitions in $LiKSO_4$ studied by EPR. Physical Review B, 45, 5163–5170.

Perrotta, A.J., and Smith, J.V. (1965) The crystal structure of kalsilite, $KAlSiO_4$. Mineralogical Magazine, 35, 588–595.

Pimenta, M.A., Echegut, P., Luspin, Y., Hauret, G., Gervais, F., and Abélard, P. (1989) High-temperature phase transitions in $LiKSO_4$. Physical Review B, 39, 3361–3368.

Rajagopal, H., Jaya, V., Sequeira, A., and Chidambaram, R. (1991) Neutron profile refinement study of the low-temperature structural phases of $LiKSO_4$. Physica, B174, 95–100.

Sahama, Th.G. (1957) Complex nepheline-kalsilite phenocrysts in Kabfumu lava, Nyiragongo area, North Kivu in Belgian Congo. Journal of Geology, 65, 515–526.

——— (1958) A complex form of natural nepheline from Iivaara, Finland. American Mineralogist, 43, 165–166.

——— (1960) Kalsilite in the lavas of Mt. Nyiragongo (Belgian Congo). Journal of Petrology, 1, 146–171.

——— (1962) Perthite-like exsolution in the nepheline-kalsilite system. Norsk Geologisk Tidsskrift, 42(2), 168–179.

Sahama, Th.G., and Smith, J.V. (1957) Tri-kalsilite, a new mineral. American Mineralogist, 42, 286.

Salje, E.K.H., Graeme-Barber, A., Carpenter, M.A., and Bismayer, U. (1993) Lattice parameters, spontaneous strain and phase transitions in $Pb_3(PO_4)_2$. Acta Crystallographica, B49, 387–392.

Sandiford, M., and Santosh, M. (1991) A granulite facies kalsilite-leucite-hibonite association from Punalur, Southern India. Mineralogy and Petrology, 43, 225–236.

Sandomirskiy, P.A., and Urusov, V.S. (1988) Phase relationships and thermal expansion for $KAlSiO_4$ polymorphs. Geochemistry International, 25, 62–73.

Schulz, H., Zucker, U., and Frech, R. (1985) Crystal structure of $KLiSO_4$ as a function of temperature. Acta Crystallographica, B41, 21–26.

Schulze, A.-R., and Müller-Buschbaum, H. (1981) Zur Struktur von monoklinem $SrAl_2O_4$. Zeitschrift für anorganische und allgemeine Chemie, 475, 205–210.

Smith, J.V., and Sahama, Th.G. (1957) Order-disorder in kalsilite. American Mineralogist, 42, 287–288.

Smith, J.V., and Tuttle, O.F. (1957) The nepheline-kalsilite system: I. X-ray data for the crystalline phases. American Journal of Sciences, 255, 282–305.

Sorge, G., and Hempel, H. (1986) Optical investigations of $LiKSO_4$ single crystals in the temperature range between 150 up to 730 K. Physica Status Solidi a, 97, 431–440.

Stebbins, J.F., Murdoch, J.B., Carmichael, I.S.E., and Pines, A. (1986) Defects and short-range order in nepheline group minerals: a silicon-29 nuclear magnetic resonance study. Physics and Chemistry of Minerals, 13, 371–381.

Stokes, H.T., and Hatch, D.M. (1988) Isotropy subgroups of the 230 crystallographic space groups. World Scientific, Singapore.

Tomaszewski, P.E., and Lukaszewicz, K. (1983) X-ray study of the low-temperature phase transitions in $LiKSO_4$. Phase Transitions, 4, 37–46.

Tuttle, O.F., and Smith, J.V. (1958) The nepheline-kalsilite system: II. Phase relations. American Journal of Science, 256, 571–589.

Varma, V., Bhattacharjee, R., Fernandes, J.R., and Rao, C.N.R. (1990) Phase transitions in $KLiSO_4$ and $RbLiSO_4$: An infrared spectroscopic investigation. Solid State Communications, 76, 627–630.

Withers, R.L., Thompson, J.G., Xiao, Y., and Kirkpatrick, R.J. (1994) An electron diffraction study of the polymorphs of $SiO_2$-tridymite. Physics and Chemistry of Minerals, 21, 421–433.

Yund, R.A., McCallister, R.H., and Savin, S.M. (1972) An experimental study of nepheline-kalsilite exsolution. Journal of Petrology, 13, 255–272.

Zhang, P.L., Yan, Q.W., and Boucherle, J.X. (1988) Crystal structure of $KLiSO_4$ at 200 K: A neutron diffraction study. Acta Crystallographica, C44, 592–595.

Manuscript received June 14, 1995
Manuscript accepted January 10, 1996